UNIVERSITY OF ILLINOIS
URBANA

AERONOMY REPORT NO. 101

AN IMPROVED PULSE-HEIGHT ANALYZER FOR ENERGETIC PARTICLE MEASUREMENTS IN THE UPPER ATMOSPHERE

by
L. Dean
L. G. Smith

February 1, 1982

Library of Congress ISSN 0568-0581

Aeronomy Laboratory
Department of Electrical Engineering
University of Illinois
Urbana, Illinois

Supported by
National Aeronautics and Space Administration

UILU-ENG-82-2501

A E R O N O M Y R E P O R T

NO. 101

AN IMPROVED PULSE-HEIGHT ANALYZER FOR ENERGETIC PARTICLE MEASUREMENTS IN THE UPPER ATMOSPHERE

by

L. Dean
L. G. Smith

February 1, 1982

Supported by
National Aeronautics
and Space Administration
Grant NGR 14-005-181

Aeronomy Laboratory
Department of Electrical Engineering
University of Illinois
Urbana, Illinois

ABSTRACT

A new Energetic Particle Spectrometer (EPS) for measurements in the upper atmosphere by rocket is described. The system has two methods of processing data. One is a staircase generator using threshold detectors; the other is a peak detector. The system incorporates a logarithmic converter for better resolution at low amplitudes and better use of telemetry channels. The circuits are described and calibration procedures are given. Modifications are recommended for high flux environments. Appendices cover sampling error in the peak detector and modifications made to the receiver of the propagation experiment.

TABLE OF CONTENTS

LIST OF TABLES

LIST OF FIGURES

1. INTRODUCTION

This report describes an improved Energetic Particle Spectrometer (EPS) developed in the Aeronomy Laboratory. The new EPS is included in the payloads of three Taurus Orion rockets launched from Kiruna, Sweden in November 1980 as part of the Energy Budget Campaign. The experiments were successful in obtaining spectrums and pitch-angle distributions, though, as will be discussed later, the data reduction has been made more difficult because of the high fluxes encountered. The same experiment is included in the payloads of two Nike Orion rockets to be launched from Wallops Island, Virginia in late 1981 and 1982*.

In the years 1972 to 1978 the effects of energetic particle precipitation at middle latitudes (represented by Wallops Island) and at the magnetic equator (at Chilca, Peru) had been investigated in terms of the measurement of fluxes directly by the use of energetic particle detectors and indirectly by the ionization produced in the nighttime ionosphere. The flights, included in Table 1.1, were mainly near midnight when ionization by scattered solar radiation is at a minimum. The experiments have been summarized and extrapolated to a global picture of energetic particle precipitation by *Voss and Smith* [1980].

In 1979 three Nike Tomahawk rockets were launched near Red Lake, Ontario, Canada in connection with the total solar eclipse of 26 February. Energetic particle detectors in the payloads of these rockets showed high fluxes in the two flights during the eclipse and in another flight on 24 February. These data are particularly valuable because of the rarity of daytime observations of energetic particles and because of the many other simultaneous and nearly simultaneous observations available for comparison. These are the subject of a report by M. K. McInerney and L. G. Smith (in preparation).

The complement of detectors in each payload is also indicated in Table 1.1. The first flight used a Geiger counter sensitive to energies > 70 keV [*Voss and Smith*, 1974]. All subsequent flights have used solid-state detectors, sometimes in pairs with different thicknesses of metal to allow discrimination

---

* The first of these, Nike Orion 31.014, was launched at 2347 EST on 13 October 1981. All experiments appear to have performed satisfactorily.

Table 1.1

Rocket launches containing particle detectors.

ROCKET*	SITE**	TIME (LST)	DATE	DETECTORS***
14.439	WI	0003	1 Nov. 1972	1 Geiger counter (1)
14.520	WI	2330	18 Apr. 1974	1 solid state (5)
14.521	WI	2120	29 Jun. 1974	1 solid state (4)
14.522	WI	2340	29 Jun. 1974	
14.523	WI	0415	30 Jun. 1974	
14.524	P	2336	29 May 1975	1 solid state (4)
14.525	P	0011	2 Jun. 1975	
14.534	WI	0001	10 Aug. 1977	1 solid state (5)
14.533	WI	0001	5 Jan. 1978	2 solid state (3 each)
14.543	WI	2315	19 Jun. 1978	6 solid state (various) with microprocessor
14.542	WI	0030	27 Sep. 1978	
18.1020	C	1052	24 Feb. 1979	2 solid state (3 each)
18.1021	C	1052	26 Feb. 1979	
18.1022	C	1054+10s	26 Feb. 1979	
33.010	S	0349+40s (UT)	16 Nov. 1980	4 solid state (1 each) with microprocessor
33.011	S	0415 (UT)	16 Nov. 1980	
33.009	S	2344+30s (UT)	30 Nov. 1980	

* Prefix 14 = Nike Apache; 18 = Nike Tomahawk; 33 = Taurus Orion

** Launch site: WI = Wallops Island; P = Peru; C = Canada; S = Sweden

*** The number and type of detectors are followed by the numbers of energy levels in the staircase generator system.

of the type of particle [*Fries et al.*, 1979], and in different orientations to increase the range of pitch angles that can be observed.

The electronics used with the solid state detectors have always included a staircase generator system which uses several threshold detectors to obtain the energy spectrum. This has been supplemented on some flights, as indicated in Table 1.1, by a microprocessor experiment which uses a peak detector to measure pulse height and then, on board the rocket, sorts and accumulates the data by energy and pitch angle. The first such system was used during the JASPIC program in 1978. An improved version of this experiment was developed for the Energy Budget Campaign and first flown in 1980.

These and other experiments used in rocket payloads since 1972 are described in detail in a series of Aeronomy Reports listed in Table 1.2. Copies of these are available on request.

The organization of this report is as follows. A general description of the new EPS system is given in Chapter 2. The staircase generator system is described in greater detail in Chapter 3 and the pulse-height analyzer in Chapter 4. The integration of these experiments into the payloads is described in Chapter 5 and their calibration in Chapter 6. Recommendations for future work are given in Chapter 7.

There are two appendices. In the first the method of correcting the data for sampling error in the peak detector is derived.

The second appendix is related not to the energetic particle experiment but to the propagation experiment. Previous to the Energy Budget Campaign the propagation experiment had involved a 500 Hz modulation of the signal [*Gilchrist and Smith*, 1979]. There already existed, at the launch site in Sweden, ground-based transmitters for a propagation experiment which uses an unmodulated signal. The modifications to the rocket-borne receiver to accommodate the unmodulated signal are described in the second appendix.

Table 1.2

Descriptions of rocket experiments contained in Aeronomy Reports.

#63 H. D. Voss and L. G. Smith [1974], Design and calibration of a rocket-borne electron spectrometer for investigation of particle ionization in the nighttime midlatitude E region.

#64 J. C. Ginther and L. G. Smith [1974], Studies of the differential absorption experiment.

#66 J. C. Evans and L. G. Smith [1975], Rocket measurements of ozone and and molecular oxygen by absorption spectroscopy.

#73 R. W. Fillinger, Jr., E. A. Mechtly and E. K. Walton [1976], Analysis of sounding rocket data from Punta Chilca, Peru.

#76 K. L. Miller and L. G. Smith [1976], Midlatitude sporadic-E layers.

#77 L. D. Paarmann and L. G. Smith [1977], A rocket-borne airglow photometer.

#78 H. D. Voss and L. G. Smith [1977], Energetic particles and ionization in the nighttime middle and low latitude ionosphere.

#80 D. E. Klaus and L. G. Smith [1978], Rocket observations of electron-density irregularities in the equatorial ionosphere.

#82 M. A. Pozzi, L. G. Smith and H. D. Voss [1979], A rocket-borne electrostatic analyzer for measurement of energetic particle flux.

#83 W. Leung, L. G. Smith and H. D. Voss [1979], A rocket-borne pulse-height analyzer for energetic particle measurements.

#84 L. L. Davis, L. G. Smith and H. D. Voss [1979], A rocket-borne data-manipulation experiment using a microprocessor.

#85 B. E. Gilchrist and L. G. Smith [1979], Rocket measurement of electron density in the nighttime ionosphere.

#91 K. L. Fries, L. G. Smith and H. D. Voss [1979], A rocket-borne energy spectrometer using multiple solid-state detectors for particle identification.

#92 R. K. Zimmerman, Jr. and L. G. Smith [1980], Rocket measurements of electron temperature in the E region.

#93 H. M. Bliss and L. G. Smith [1980], Rocket observations of solar radiation during the eclipse of 26 February 1979.

Table 1.2 (Continued)

#95 C. Durkin and L. G. Smith [1981], A rocket-borne Langmuir probe for high resolution measurement of the ionospheric electron temperature profile.

#96 F. M. Braswell and L. G. Smith [1981], A rocket-borne microprocessor-based experiment for investigation of energetic particles in the *D* and *E* regions.

2. GENERAL DESCRIPTION OF THE SYSTEM

2.1 *Introduction*

The Energetic Particle Spectrometer (EPS) measures the flux and pitch angles of the particles and determines their type (electron, proton, heavier ion). Four detectors are used. Two systems are used for presenting the data. In one, the staircase generator system, the information is transmitted in real time. In the other system, which uses a microprocessor, the data are sorted and accumulated for about 5s before transmission.

A block diagram of the entire EPS system is shown in Figure 2.1. The output of each of the four detectors is amplified (in the preamplifier), shaped, and then further amplified. The resulting signals are then processed in the two parallel paths already mentioned. One signal path consists of the threshold detectors and staircase generators, contained on the Staircase Generator Card, which also includes the amplifiers. A block diagram of the staircase generator system is shown in Figure 2.2

The staircase generator counts the total number of pulses received above a threshold level from each of the four shapers (one for each of the four detectors). The output for each channel is a 0-to-5 V staircase with 32 counts in each staircase.

Each of the inputs uses a Datel AM 462-2 operational amplifier. This op amp has 80 V/μs (minimum) slew rate and 200 ns settling time, and accurately reproduces the input pulse. The circuit board is built so that either the inverting or non-inverting mode may be used, depending on whether the detectors use aluminum or gold coatings.

The detector, preamplifier, and shaper give a nominal 100 mV peak positive pulse with a 116 keV particle. It is desired to measure to 128 keV. The corresponding input to the PHA with a 128 keV input is to be -5 V. Therefore the nominal desired voltage gain for the first amplifier is -5/0.11 = -45. The exact gain is set by choice of feedback resistors so that with the staircase generator connected to the specific detector, preamplifier, and shaper to be used in the flight, the 116 keV line from a Co-57 source will give a -4.53V peak pulse out of the first staircase generator amplifiers. The output from each amplifier is fed to a threshold detector set so that the staircase generator will not be exposed to noise in the absence of a pulse. The threshold detectors are set for a threshold of -0.94 V

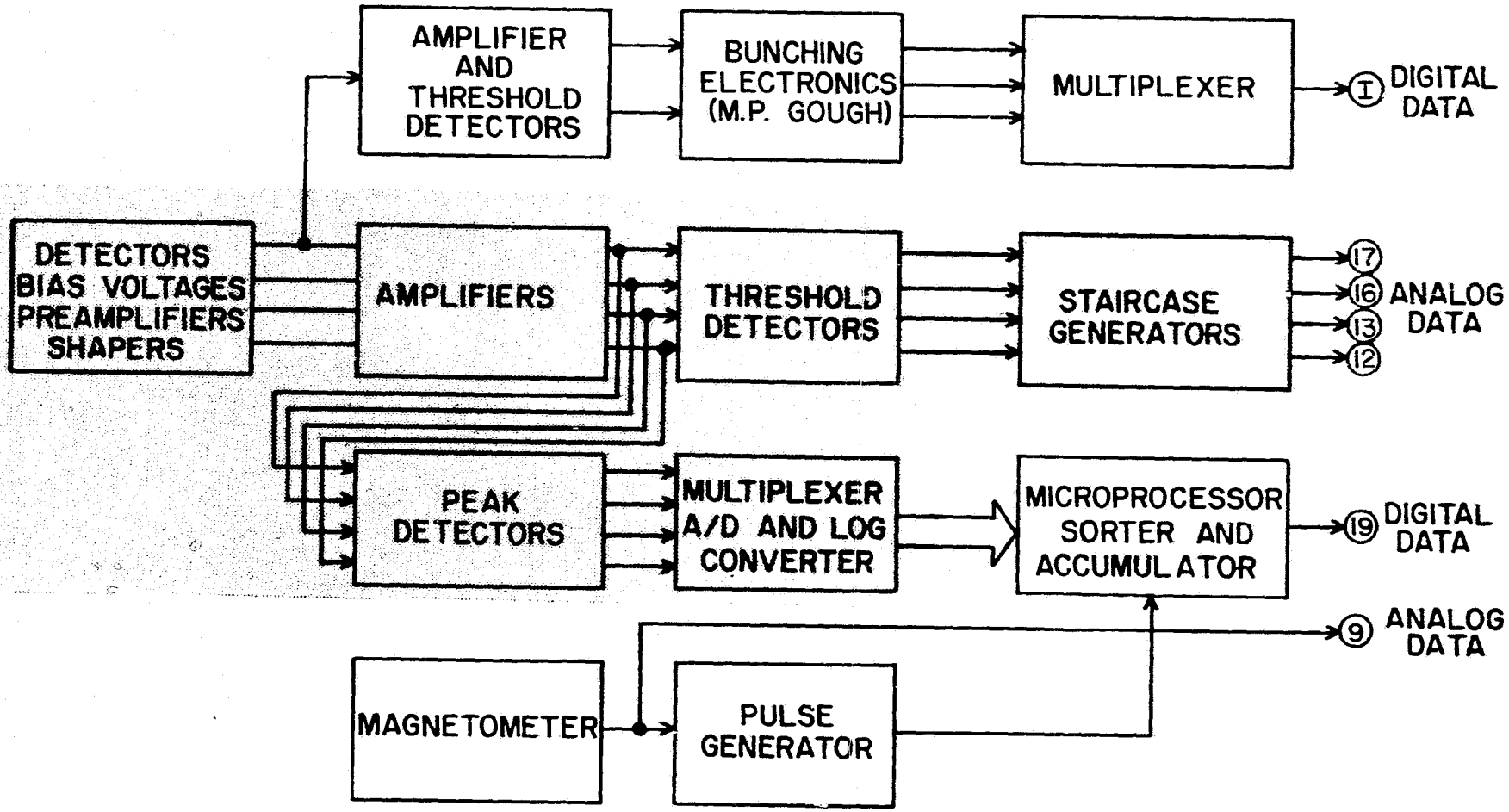

Figure 2.1 Block diagram of the energetic particle spectrometer used in the Energy Budget Campaign. The shaded area indicates the circuits described in detail in this report.

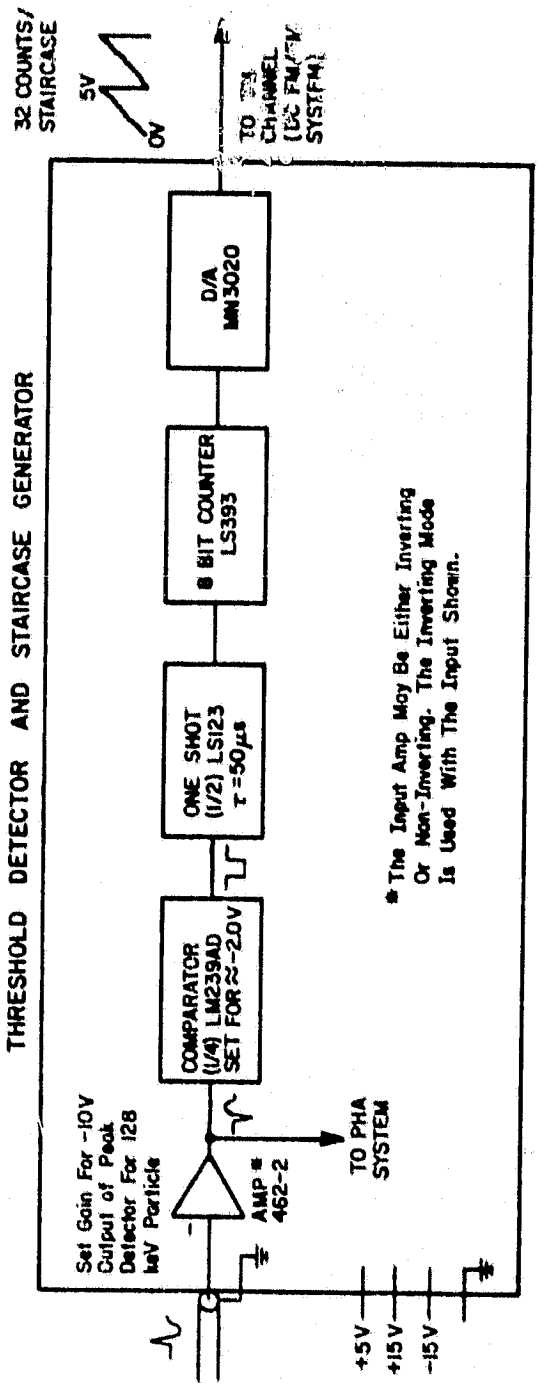

Figure 2.2 Block diagram of one of the four channels of the staircase generator system.

which corresponds to an energy level of approximately 24 keV.

The pulses that are only slightly greater than the threshold have substantial noise modulation which could cause multiple counts. Therefore a one-shot with a 50-μs period is used. At high count rates this dead time causes an appreciable counting error but since the pulses are Poisson distributed, it can readily be corrected [*Voss and Smith*, 1974]. The number of pulses from the one-shot are counted with a ripple counter, and the counter's states are fed to a D/A converter. The D/A has an output of 0 to 5 V, appropriate for the VCO's of the FM/FM telemetry system.

The other signal path, shown in Figure 2.1, is through the peak detectors, the multiplexer and log converter, and the microprocessor. The part of the system from the peak detectors to a first-in-first-out (FIFO) memory is situated on the Pulse-Height Analyzer (PHA) Card. A block diagram of the PHA is shown in Figure 2.3. The PHA sequentially samples each of the four inputs for 180 μs every 200 μs and gives a four-bit parallel output proportional to the log of the strongest pulse sampled in each sector during the preceding 200 μs. It also simultaneously sends 2 bits showing the sector sampled.

The peak detector of the PHA is the LM 318. This high-speed op amp is followed by a diode rectifier. The device is connected as a non-inverting amplifier with a voltage gain of 2 and therefore the output capacitor will be charged to twice the most negative level applied to the input. Since the input is a negative pulse, the capacitor will be charged to a negative voltage linearly proportional to the magnitude of the particle energy. The amplifier output impedance and the capacitor are small so that the capacitor can become essentially fully charged with a short pulse.

The peak detectors are followed by the multiplexer. The multiplexer (MN7100) is a selector, S/H and A/D, all in one package. It is controlled by logic operating from the system clock. It has an 8-bit parallel output (7 significant bits plus the sign). It can take a ±20 V input, but is calibrated for 256 intervals over ±10 V (128 intervals over our range of 0 to -10 V).

A discharger is also connected to the peak detector. After the peak value is read by the multiplexer, the discharger shorts out the peak detector's capacitor. It uses a MOSFET having a saturated impedance

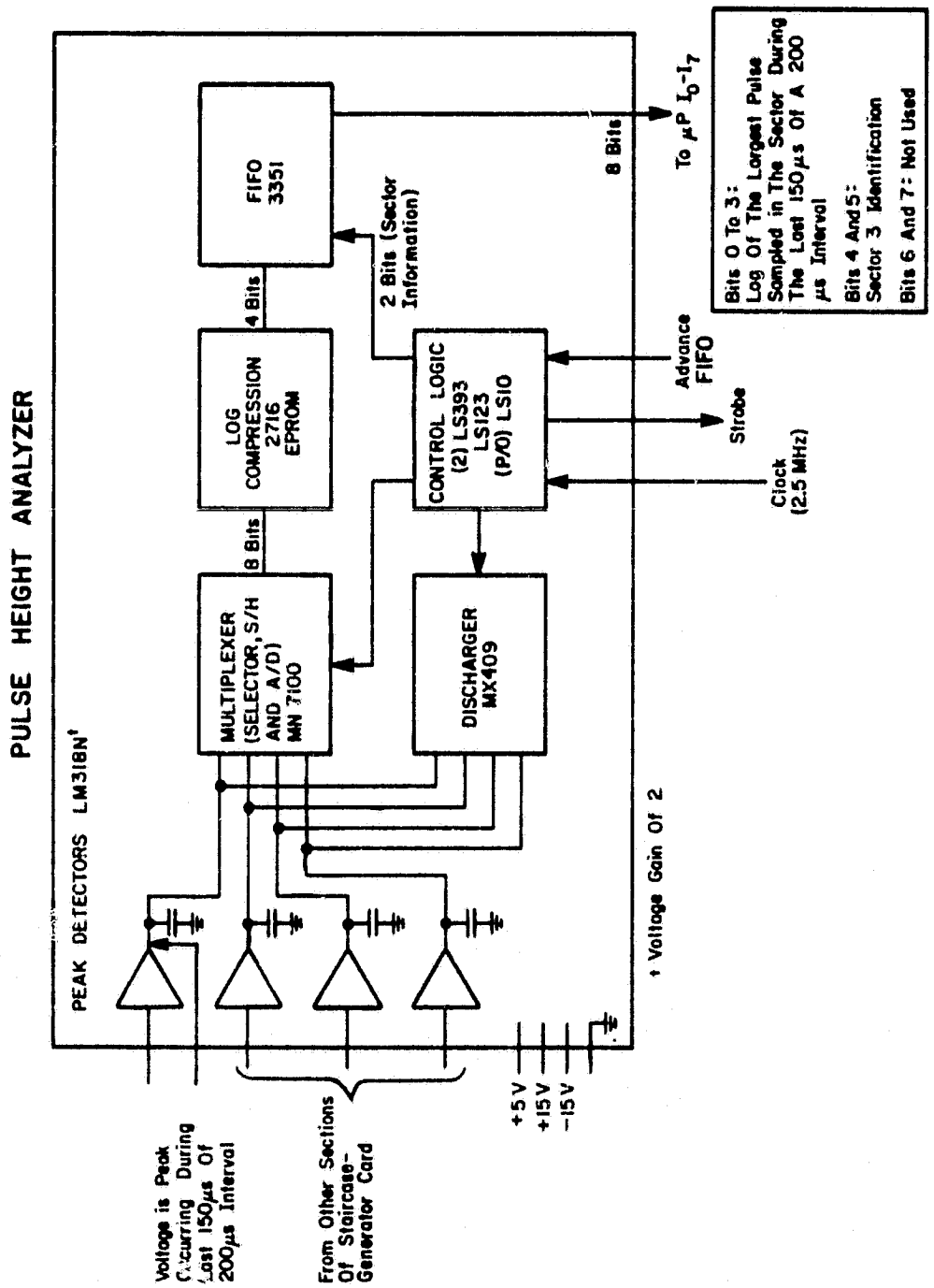

Figure 2.3 Block diagram of the pulse-height analyzer system.

of 2 kΩ. Since the output impedance of the peak detector will be much less than 2 kΩ, a pulse arriving during the discharge time will still be momentarily seen.

The log of the output of the MN7100 is taken for better relative energy resolution (as discussed later). The output of the PHA is fed into the microprocessor which compresses the magnitude and pitch-angle data so that more information can be sent over the telemetry channel's limited bandwidth.

Since the microprocessor may not be ready for data when the log converter puts it out (the microprocessor may be on an interrupt), the log converter's output together with the appropriate detector information is fed into a FIFO memory. When the microprocessor is ready for the data, it advances the FIFO output.

The rest of this chapter briefly discusses the first block in Figure 2.1 (i.e. the detectors, preamplifiers and shapers) and how the circuit in the shaded area differs from the previous EPS system. The following two chapters describe the staircase-generator card and the PHA card in detail. The microprocessor system is described in *Braswell and Smith* [1981].

2.2 *Energetic Particle Detectors*

The detectors are silicon surface-barrier devices. They have a sensitive area of 50 mm^2 and a depletion layer thickness of 300 μm. All of those used so far have an aluminum layer on p-type silicon and are operated with a negative reverse bias of 90 V. Other detectors are made by putting gold on n-type silicon; these require a positive reverse bias. All of the units are made by Ortec, Inc. The bias voltage is supplied from a battery through a 10 MΩ resistor (R1) in the preamplifier, Figure 2.4.

An energetic particle striking a diode generates electron-hole pairs in the depletion layer. These are rapidly dispersed by the high electric field. The amount of charge is linearly proportional to the energy of the particle. Since the bias source has a high impedance, the charge is deposited on the input capacitance of the preamplifier. A 50 keV particle causes approximately a 9 μV pulse at the preamplifier input. The detectors are discussed in *Voss and Smith* [1974].

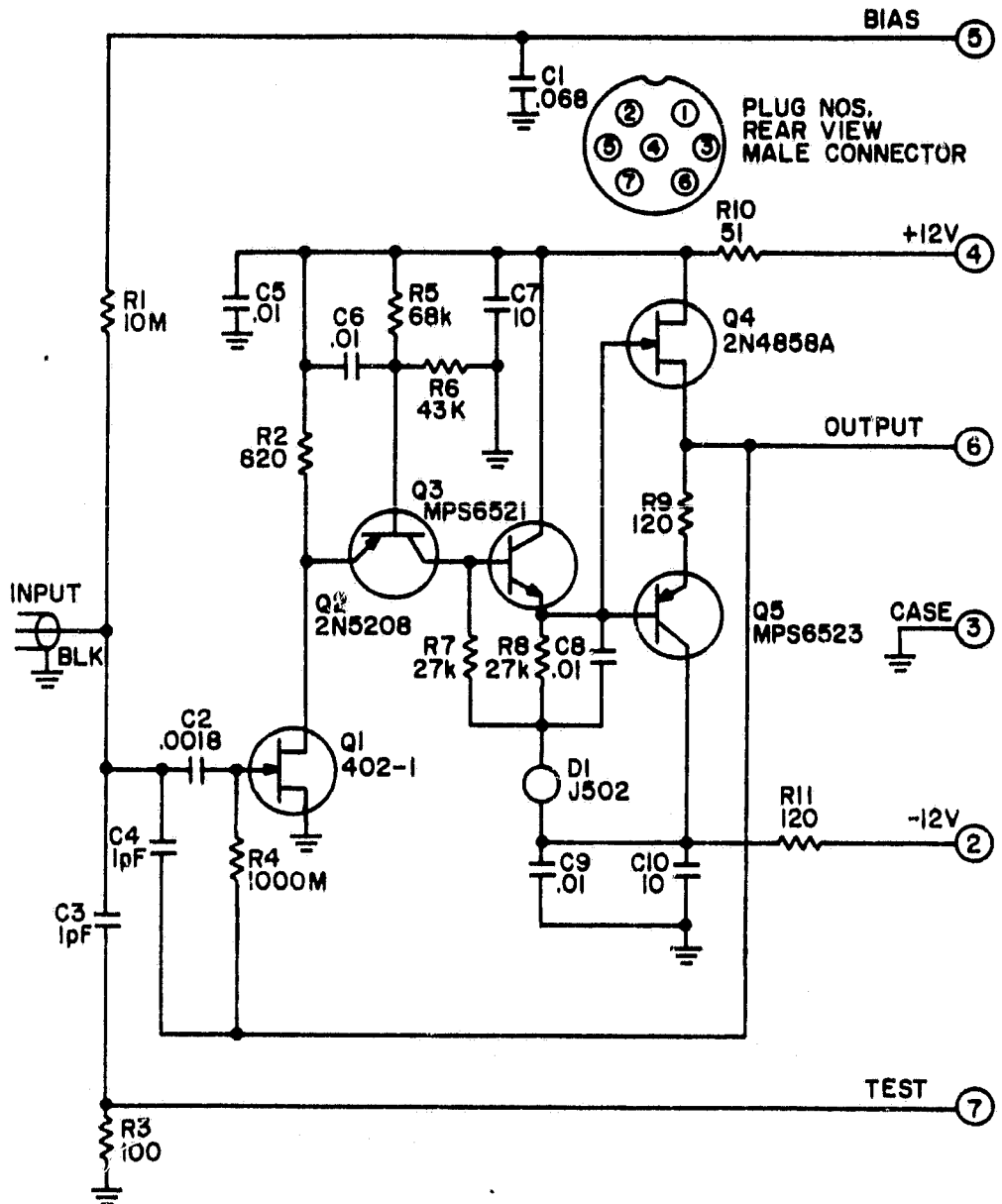

Figure 2.4 Circuit diagram of the preamplifier: Nucleometrics Model 402.

2.3 *Charge Preamplifier*

The preamplifier used is a Nucleometrics model 402. This circuit is shown in Figure 2.4. The preamplifier is a very low noise-figure amplifier (connected as an integrator) whose output voltage is a staircase, where the magnitude of a step is linearly proportional to the charge deposited on its input capacitance (C2).

Since a negative bias is used on the detectors (with the type of detectors used on these flights) the pulse of current in the detector causes the detector voltage to momentarily move toward zero, so the input of the preamplifier goes more positive and current is injected into the preamplifier. Q1 is selected for low noise figure and is an n-channel junction FET, similar to the 2N4417. In the steady state, the output of the preamplifier is negative so that the feedback through R4 causes Q1 to conduct at about 8 mA. The injected current from the detector due to an energetic particle charges C1 which causes Q1 to conduct more which decreases the conduction of Q2 and Q3. Since D1 maintains a constant current sum through R7, R8 and the base of Q5, Q5 conducts more which drives the output more negative. The negative output feeds back through R4 and C4 and slowly discharges C2. Since the ac component of voltage on C2 is so small, a very small fraction of the time constant of $R4 \cdot C2 = 1.8$ s is required for this discharge, but the discharge time is much greater than the charge time so the preamplifier output is essentially a step. If a detector with positive bias is used, the voltage and current changes would all be opposite to that discussed above.

The preamplifier's quiescent point is determined by the dc feedback through R4. The error detector is Q2.

Discussions of the preamplifier's noise performance are in *Voss and Smith* [1974] and *Fries et al.* [1979].

2.4 *Pulse Shaping*

From communications theory, for a signal and "white" Gaussian noise the optimal linear filter has an impulse response which is the mirror image of the desired signal fed into it. However, the shaper's input noise is not white since an appreciable amount of the preamplifier's noise varies a $1/\omega^2$. Therefore, the first stage of the shaper is a pre-whitening filter: that is, it is one whose gain is a function of

frequency in such a way that its output noise, when fed by the preamplifier, is "white" (constant with frequency). The prewhitening stage alters the shape of the desired signal. The altered signal response is a sum of a positive step function and an equal magnitude negative exponential. The mirror image of the impulse response of the altered signal is anticipatory or noncausal, so it cannot be physically realized. However, many filters can be designed which approach the optimal filter in performance. A $(CR)^{1} \cdot (RC)^{3}$ unit was developed and is described in *Fries et al.* [1979]. A slightly modified shaper as shown in Figure 2.5 was used. The shaper equivalent circuit and output waveform are shown in *Leung et al.* [1979: Figures 4.5 and 4.6].

Since the shaper stretches the input waveform, an error can occur if one pulse begins before the preceding pulse has decayed. This problem was called "pile up" in *Fries et al.* [1979] and is separate from the distortion of the energy spectrum due to peak detection (discussed later). Using Fries' approach, the probability that two or more counts will occur within a 15 μs interval with 10^{4} counts s^{-1} is only 1% while there is an over 13% chance that one pulse will occur. Therefore, pile up begins to become important at the high count rates.

2.5 *Comparison of the New EPS System with the Previous System.*

2.5.1 *The previous staircase generator configuration.* Prior to the JASPIC project (1978) all EPS data were obtained only from staircase generators in a voltage discriminator circuit. The circuit used is shown in detail in *Voss and Smith* [1974: Figure 5.20]. The circuit employs several voltage comparators where each comparator is referenced to a different voltage. Due to the amount of circuitry and number of telemetry channels required usually only three levels from one detector were measured on any one payload. The levels were, nominally, E>25 keV, E>40 keV and E>70 keV up to, and including, the JASPIC program. On the 1979 eclipse flights are Red Lake, Ontario, Canada, levels of E>40 keV, E>70 keV, and E>100 keV were used.

2.5.2 *The Pulse-Height Analyzer.* The use of the PHA allows the elimination of much of staircase generator circuitry and a reduction in the

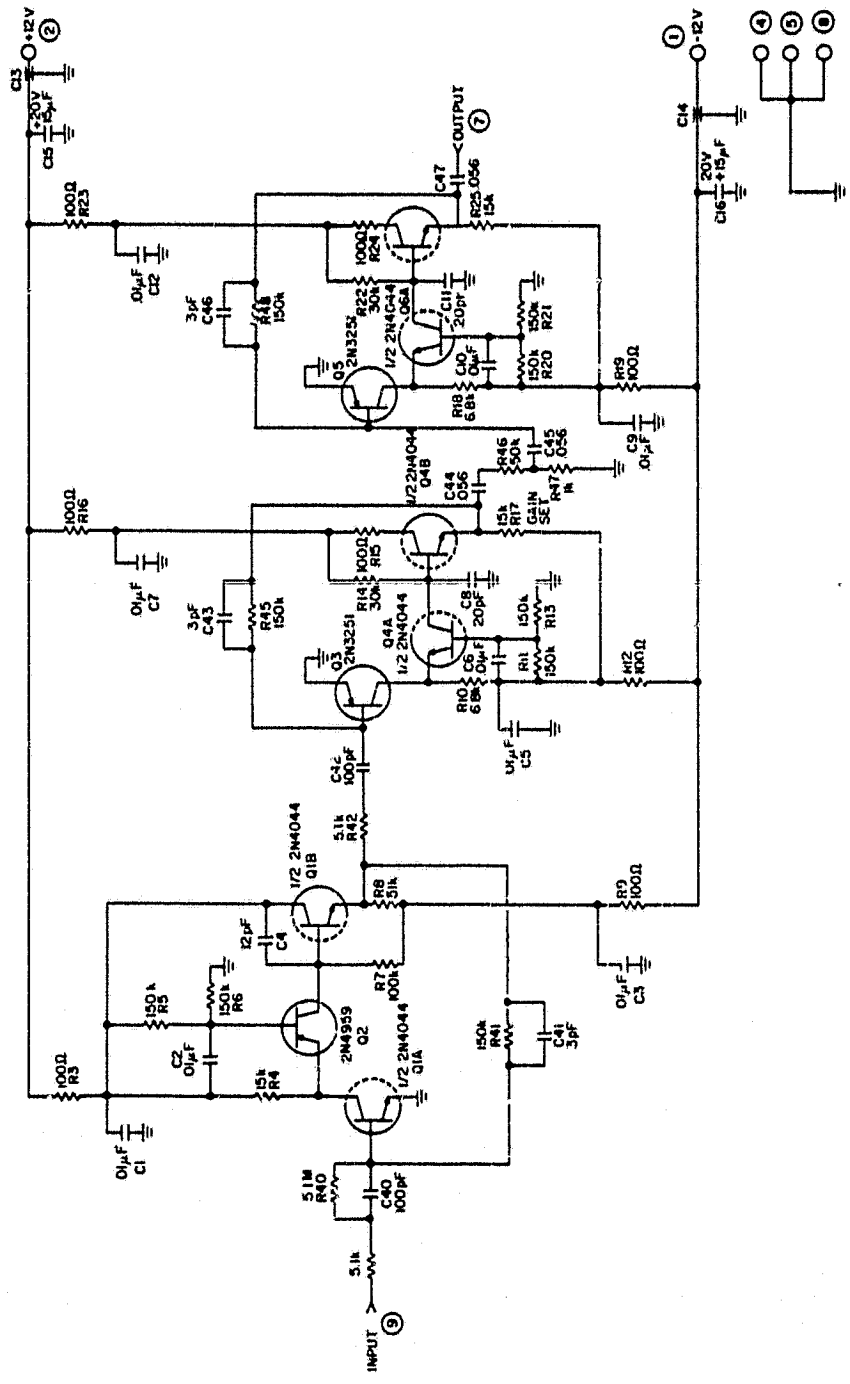

Figure 2.5 Circuit diagram of the pulse shaper.

telemetry channel requirements for EPS measurements. The PHA shown in Figure 2.6 was used in the JASPIC Program. The first half of the present PHA is functionally similar to the previous PHA, but the availability of a high-speed multiplexer, sample-and-hold, and analog-to-digital converter in one hybrid integrated circuit (the MN7100) has allowed the new circuit to be built in about half the space.

The sample-and-hold used in the original PHA provided a back up to the microprocessor system. Even though one of the widest telemetry channels was used, the data rate required to transmit all the data without processing was too great for the telemetry channel. Therefore, the sample-and-hold was synchronized to the multiplexer so that only every fifth pulse was read out. Therefore, only 20% of the data obtained from the microprocessor system was available through the back-up system.

The old peak detector had a quiesient output of -1 V. While this did not apparently cause any real problems, it was eliminated in the newer system by a true peak detector. A high speed amplifier was also used to more accurately respond to the peaks.

2.5.3 *The logarithmic converter.* A substantial functional difference between the old and new PHAs is the addition of the logarithmic converter. Although the multiplexer has a nominal resolution equivalent to 1 keV, the microprocessor only has enough memory to accommodate 4 bits of magnitude information (16 levels). The telemetry channel would also need a greater bandwidth to handle more than 4 bits of magnitude information. This reduces the system resolution to 8 keV. In order to achieve a constant percentage resolution rather than a constant absolute resolution, a log converter follows the multiplexer. The log converter increases the system's absolute resolution at low magnitudes at the expense of absolute resolution at high magnitudes.

The advantage of using the log converter is illustrated in Table 2.1. The 16 output levels are derived from 128 input levels, where each input level may be 1 keV, for example. Assuming input levels from 0 to 14 (i.e. energies $\leq$ 14 keV) contain only noise, these are assigned to output channel 0. Input channel 15 contains all energies $\geq$ some specified value (in our example 127 keV). The remaining intervals are divided on a linear or a logarithmic scale.

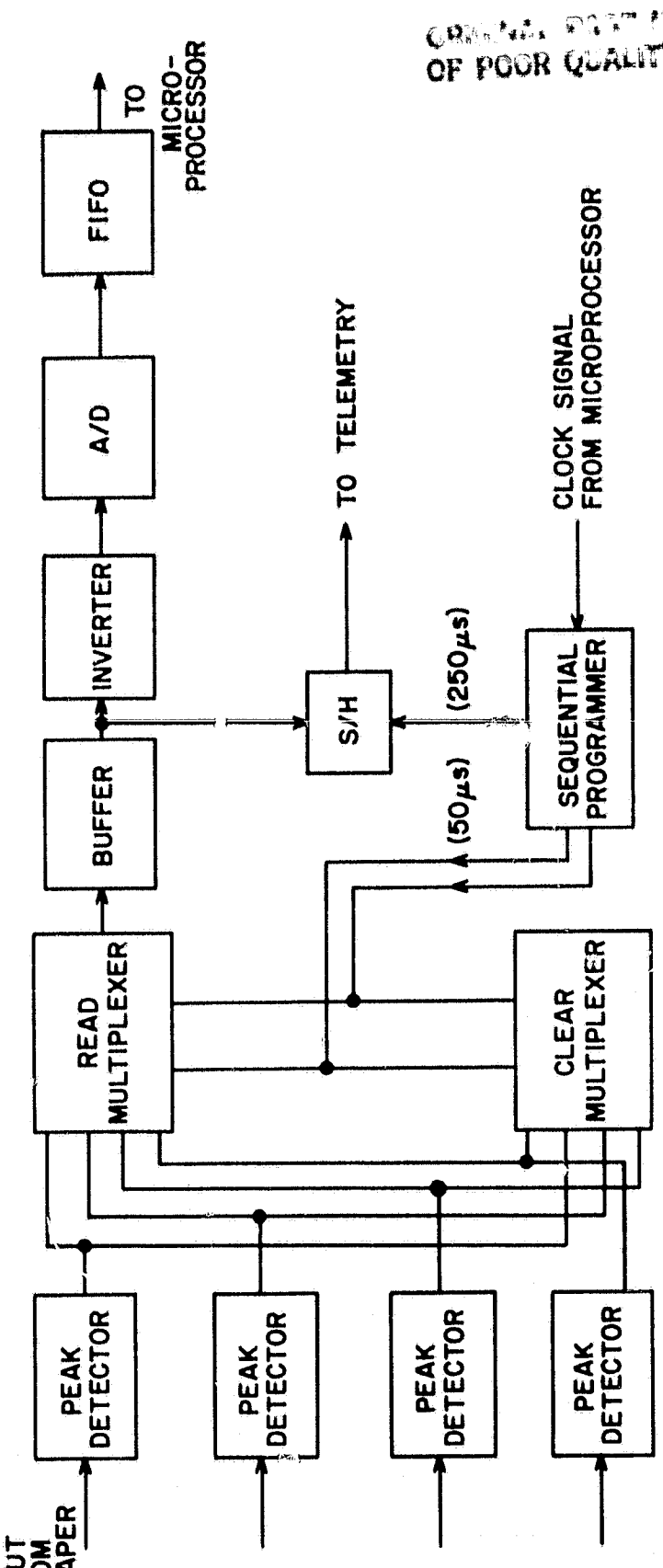

Figure 2.6 Block diagram of the pulse-height analyzer used in the JASPIC Program.

Table 2.1

Comparison of the energy ranges obtained without and with logarithmic compression of the pulse-height data. The input is in units of keV.

OUTPUT DATA	INPUT (LINEAR)[1]	INPUT (LOGARITHMIC)[2]
0	0 - 14	0 - 14
1	15 - 22	15 - 16
2	23 - 30	17 - 19
3	31 - 38	20 - 22
4	39 - 46	23 - 26
5	47 - 54	27 - 31
6	55 - 62	32 - 36
7	63 - 70	37 - 42
8	71 - 78	43 - 49
9	79 - 86	50 - 57
10	87 - 94	58 - 67
11	95 - 102	68 - 79
12	103 - 110	80 - 92
13	111 - 118	93 - 108
14	119 - 126	109 - 126
15	127 - ∞	127 - ∞

[1]Without logarithmic compression

[2]With logarithmic compression

Notice that output channels 1 and 2 contain the energy ranges, for the linear scale, of 15 to 22 keV and 23 to 30 keV, together covering a factor of 2 in particle energy. For the logarithmic scale these channels contain the energy ranges 15 to 16 keV and 17 to 19 keV. Because of the exponential nature of the expected energy spectrum, with the differential flux (i.e. per keV) decreasing with increasing energy the logarithmic scale will allow comparable total counts in each energy interval. Also for calculations of ionization rate the spectrum must be known with relatively greater accuracy at the lower energies.

2.5.4 *The preamplifier.* The preamplifier used in the JASPIC program is shown in Figure 5.3 of *Fries et al.* [1979]. The principal differences between the current units and the older ones are: (1) replacing the current source Q1 with simple resistors (for size and cost reduction); (2) changing the output to a complementary configuration; (3) removing the 5.1 kΩ output resistor; and (4) changing the value of C5. The unmodified Nucleometrics preamplifiers had a 0.01 μf capacitor for C5. The amplifier had the undesirable feature that, if any disturbance in the bias network occurred, it took five minutes for the circuit to recover (referred to as "bias voltage paralysis time" by Nucleometrics). Since this is unacceptable in a brief rocket flight, C5 was changed to 1800 pF.

In the eclipse flights and all flights prior to JASPIC, a combined preamplifier and shaper were used as shown in Figure 5.9 of *Voss and Smith* [1974].

2.5.5 *The shaper.* The shaper used in JASPIC is shown in Figure 5.14 of *Fries et al.* [1979] except that a μA 715 op amp was used in place of Q7a and Q7b. The output impedance of the shaper was too high, so in the current configuration both of the last two stages (Q7a and Q7b) were removed and the gain placed in the first stage of the staircase generator card. This worked satisfactorily, but the decreased signal-to-noise ratio due to pick-up on a low signal level line between the shaper and staircase generator raised the lower limit of measurement amplitude capability.

Since the new preamplifier does not have the 5.1 kΩ output resistor and the shaper depends on that source impedance for its pre-whitening function, a 5.1 kΩ resistor was added to the input of the shaper card. The analog switch on the input was also eliminated.

3. STAIRCASE GENERATOR

The staircase generator card counts the total number of pulses received above a threshold level from each of the four shapers (one for each of the four detectors). The output of each channel is a 0 to 5 V staircase with 32 counts per staircase. The staircase generator schematic is shown in Figure 3.1

3.1 *The Amplifiers*

The input of each channel of the staircase generator card is a Datel AM 462-2 wideband operational amplifier. This high speed circuit amplifies the pulse with great accuracy. It also buffers (isolates) the shapers from the remaining circuitry. The stage also allows gain adjustment to be made and may be either used in the inverting or non-inverting mode.

With the feedback as designed (i.e. without the feedback capacitor, but with the gain resistors and compensation used in the flights), the amplifier has a constant gain from dc to about 300 kHz. This permits the output to accurately follow the input pulse waveform.

The 10 pF feedback capacitors were added in the field on the units flown so far. The capacitors reduce the high frequency gain and eliminate what appears to be high frequency ringing (but is really ground-induced pick-up seen when using the module on an extender card). The capacitors are undesirable. The amplifier output should be viewed with the PC boards plugged directly into the card cage.

The staircase generator card is driven by the four shapers. The polarity of the pulses out of the shapers depends on the type of detectors used. On all flights to date, aluminum detectors have been used and a positive pulse is generated by the shaper. Since a negative pulse is needed for the threshold detectors, the amplifier is connected in the inverting mode as shown in Figure 3.1. If gold detectors are used, the amplifier would be connected in the non-inverting mode. To do this, the input is connected to the amplifier non-inverting input (pin 3) rather than to the resistor shown and what becomes the open end of the input resistor is connected to ground. Any combination of aluminum and gold detectors can be used provided that the corresponding amplifiers are wired accordingly. If an apogee switch is used to change detectors, as in JASPIC, both of the detectors must be of the same type.

ORIGINAL PAGE IS
OF POOR QUALITY

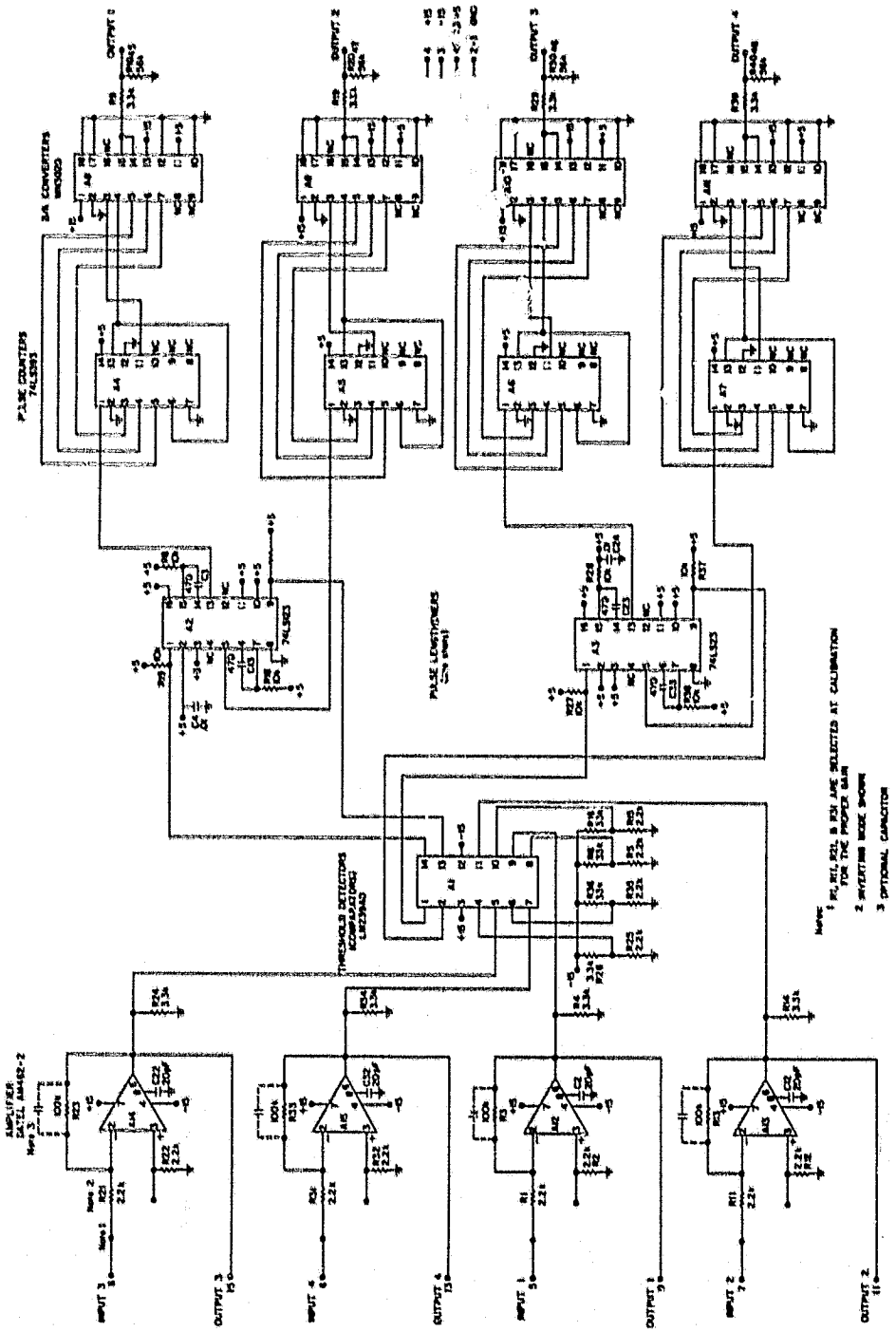

Figure 3.1 Circuit diagram of the staircase generator.

Since the gain of the preamplifier, shaper and the peak detector (of the PHA) may vary from unit to unit the gain adjustment is made in the first amplifier in the staircase generator since it is used for both EPS signal paths: R1, R11, R21, and R31 are selected at calibration for the desired gain. For all flights to the present 2.2 kΩ resistors have been used.

3.2 *The Threshold Detector*

The negative-going pulses from the amplifier are fed to one of the four sections of the LM239AD comparator, which is used as a threshold detector. The threshold detector prevents the remainder of the staircase generator card from being exposed to noise (in the absence of a pulse) which, in turn, minimizes false counts. The comparator is essentially an operational amplifier where the signal is applied to the non-inverting input and the inverting input is tied to a negative dc reference voltage. The reference (threshold) voltage is obtained through voltage dividers. The comparator differs from a conventional operational amplifier circuit in that no feedback is supplied and, rather than having a complementary output stage that can either deliver or sink current at any operating point, the comparator's output is an open collector of a very low current limited NPN transistor. The transistor's emitter is referenced to the negative supply voltage. The output transistor conducts whenever the input goes more negative than the reference. This condition momentarily grounds the input to the corresponding one shot.

The values of the voltage divider resistors are picked at calibration. Figure 2.1 shows the values used on all units flown to date.

3.3 *Pulse Lengtheners*

The pulses only slightly above the threshold have substantial noise modulation which could cause multiple counts. Therefore, a one shot with a 50 μs period is used. Some pulses will be missed, but due to the Poisson distribution of the count intervals, this can be readily compensated for as in section 5.3.3 of *Voss and Smith* [1974].

3.4 *Counter and D/A Converter*

The outputs of the one shots are connected to conventional counters. Each of the counters is connected as a pair of cascaded 4 bit binary counters. Therefore, they count through 256 steps.

The D/A converter is a MN3020. The block diagram of this converter is shown in Figure 3.2. The unipolar positive mode is used; that is, the output varies from 0 V with all zeros in to 9.961 V with all ones in. However, the converter's MSB (pin 2) is grounded so the converter output is limited to the range from 0 to 5 V.

The converter is fed so that its 5 next most significant bits are from the counter's 5 least significant bits. This gives 32 steps/staircase. By rewiring the interconnections between the counter and D/A converter, 64, 128, or even 256 steps per staircase are obtainable. The various possible interconnections are indicated in Figure 3.3. If a 256-step staircase is used, the output voltage divider must be changed so that the telemetry VCO only sees a signal in the range 0 to 5 V.

The use of a very high number of counts per staircase allows very high count rates to be handled with low telemetry channel bandwidths, but reduces resolution.

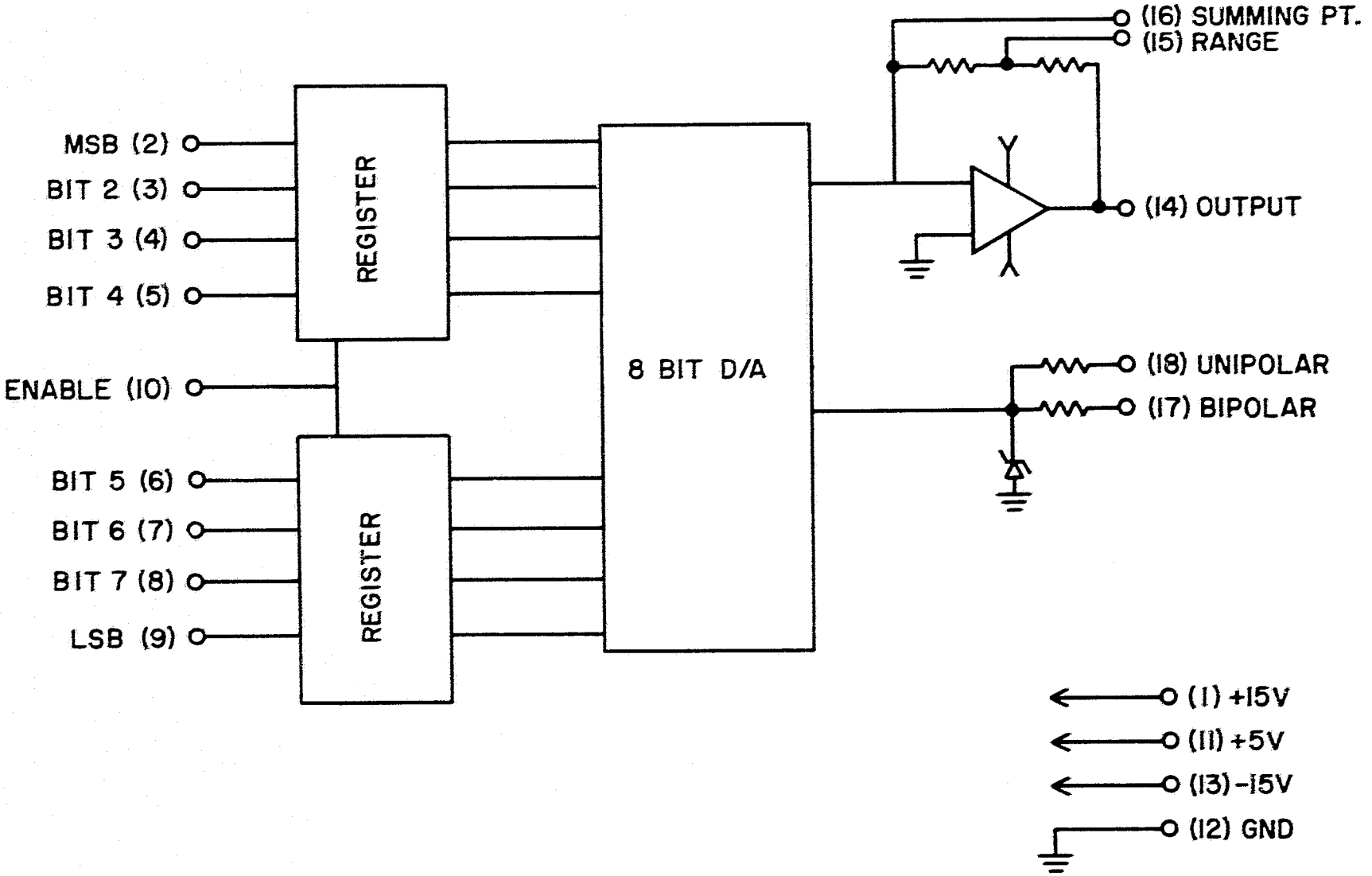

Figure 3.2 Block diagram of the MN3020 D/A converter. The pin numbers are shown in parentheses.

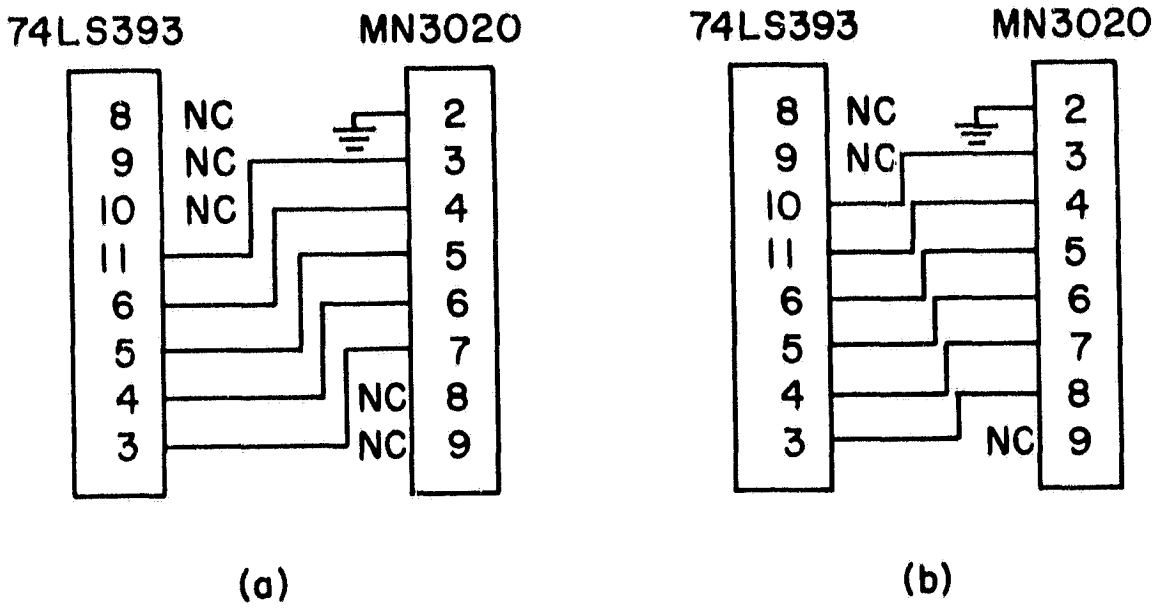

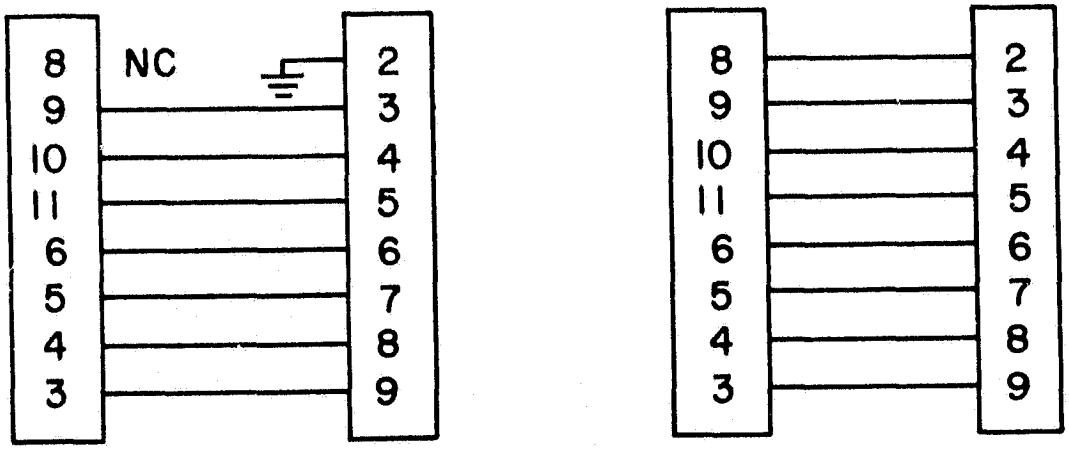

Figure 3.3 Optional interconnections between the 74LS393 counter and the MN3020 D/A for: (a) 32 counts/staircase, (b) 64 counts/staircase, (c) 128 counts/staircase, and (d) 256 counts/staircase.

4. THE PULSE-HEIGHT ANALYZER (PHA)

The pulse-height analyzer sequentially samples each of four inputs for 180 μs out of every 200 μs and gives a four-bit parallel output proportional to the log of the strongest pulse sampled in each sector during the last sampling period. It also simultaneously sends 2 bits showing the sector sampled. Figure 4.1 shows the schematic of the PHA.

4.1 *The Peak Detector*

The peak detector consists of a high-speed amplifier and a rectifier. The amplifier is a LM318 high-speed operational amplifier. The amplifier must drive a capacitive load. This operational amplifier, like most operational amplifiers, is unstable if it directly drives a capacitive load. If the amplifier is so connected, its response to a step function is a step superimposed on an oscillation of approximately 10 MHz until the capacitor is essentially fully charged. The oscillation will then cease. To prevent the oscillation, a 100Ω isolation resistor is placed between the amplifier output and the rectifier. Then, in order to avoid having a series resistor that the capacitor must charge through, the amplifier's feedback is taken after the 100Ω resistor. With the 100Ω resistor so placed in the amplifier's loop there is only a small increase in the output impedance of 0.01 ohm. The final output impedance is about 1Ω.

The resulting charging time constant is 5 ns. The shaper (section 2.4) stretches the pulse to about 300 ns. This allows 60 time constants to charge the capacitor.

A Hewlett-Packard type 5082-2800 (1N5711) hot-carrier diode is used for the rectifier to minimize voltage drop. At 25°C the typical hot-carrier diode has a voltage drop of only 0.21 V at 10 mA. Since the capacitor has time to become essentially fully charged, as discussed above, its current drops to a very low value and the low diode voltage drop allows the capacitor to fully charge. In addition, the diode has a very low reverse conduction. At 25°C it only conducts 2 nA with 5 V of reverse bias, so the capacitor remains fully charged.

4.2 *The MN7100 and the Start-Convert Generator*

The Micro Networks Laboratory MN7100 is a multiplexer, sample-and-hold and analog-to-digital converter in one hybrid package. A block diagram of

ORIGINAL PAGE IS
OF POOR QUALITY

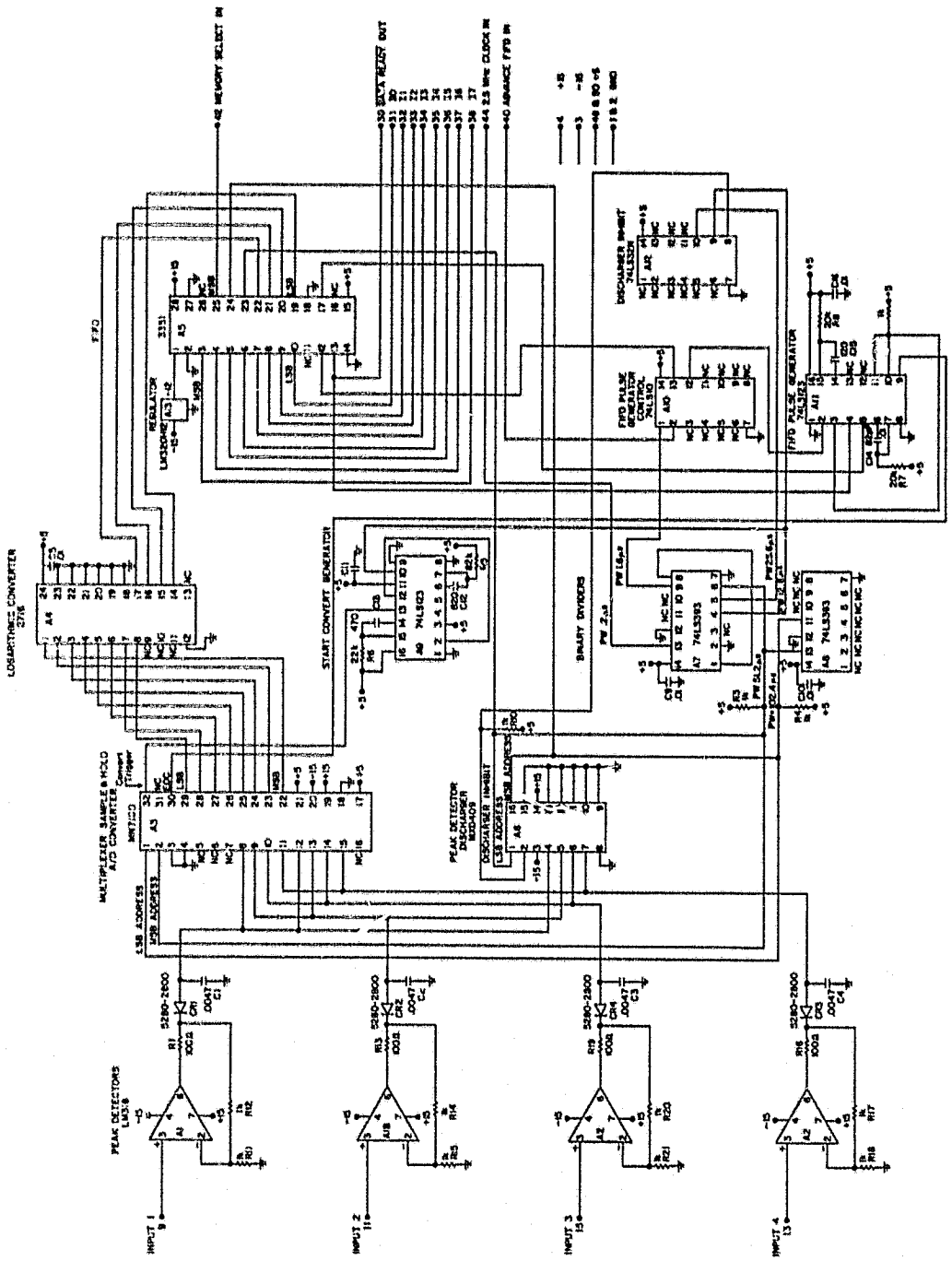

Figure 4.1 Circuit diagram of the pulse-height analyzer.

the MN7100 is shown in Figure 4.2. It sequentially samples each of the four peak detectors and converts the voltage for each detector to an 8-bit digital code consisting of 7 significant bits plus the sign.

The MN7100 is controlled by two address lines (which select the input line to be measured) and by a convert-trigger line. The address lines are divided down from the clock. The MSB address line has a pulse width of 102.4 μs while the LSB address line has a pulse width of 51.2 μs. Both address lines are square waves since they are obtained from binary counters.

Figure 4.3 shows a timing diagram for the MN7100 and the start-convert generator. The trigger line locks the MN7100 input onto the peak detector whose address is present when the trigger line goes high. The address line must have been stable for at least 100 ns before the trigger goes high. To ensure that this last condition is met, the waveform of double the frequency of the LSB address is fed to the input (pin 10) of A9. A9 is a dual one shot which is connected so that it triggers on the rising edge of its input. Since it is fed with twice the LSB address frequency, a rising edge occurs at the beginning of each change of state of the LSB address (and nowhere else).

The first one shot generates a 20 μs positive pulse on pin 12 of A9. This is certainly more than the 100 ns delay required by the MN7100. The output of this first one shot is fed to the input of the second one shot. The second one shot is triggered by the falling edge of the first one shot. The second one shot generates a 4 μs positive pulse which is the trigger pulse. This is several times the 100 ns wide pulse required by the MN7100 for the trigger. The rising edge of the trigger pulse freezes the input selector of the MN7100, as stated before, and the MN7100's sample-and-hold begins to operate on the falling edge of the trigger pulse. After approximately 5 μs the MN7100 puts out a high on the end-of-convert (EOC) line which signifies that the sample-and-hold capacitor is fully charged. The MN7100 then proceeds to digitize the sample-and-hold voltage and applies the result to its output terminals. When this process is complete, the MN7100 pulls the EOC line low. The conversion time (i.e. the time that the EOC line is high) is specified at 7 μs maximum. The total time after the new address is selected until the MN7100 starts to digitize the sample is 29 μs. Discharging must not begin until after this time.

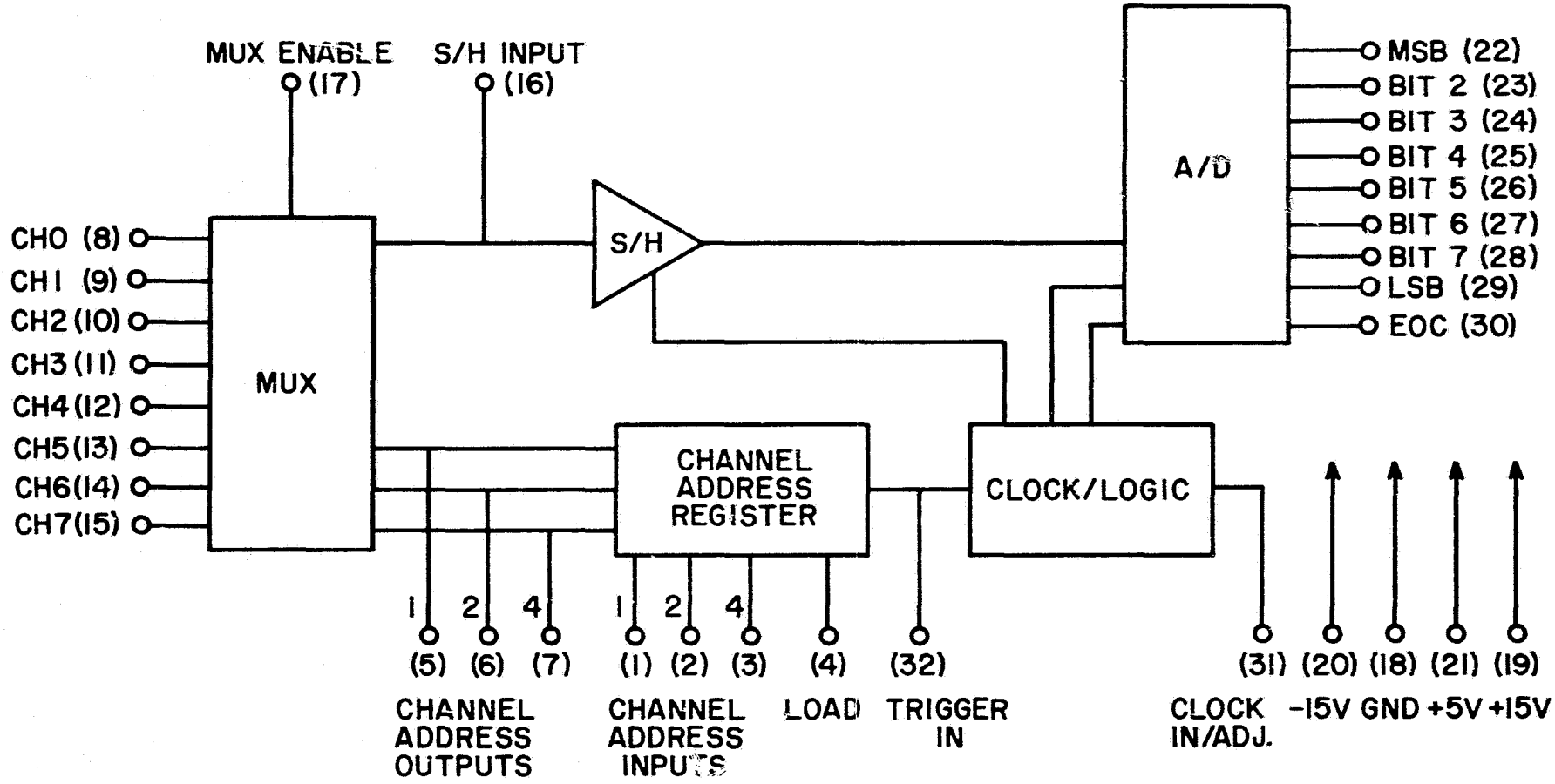

Figure 4.2 Block diagram of the MN7100 showing the multiplexer, S/H and A/D. The pin numbers are shown in parentheses.

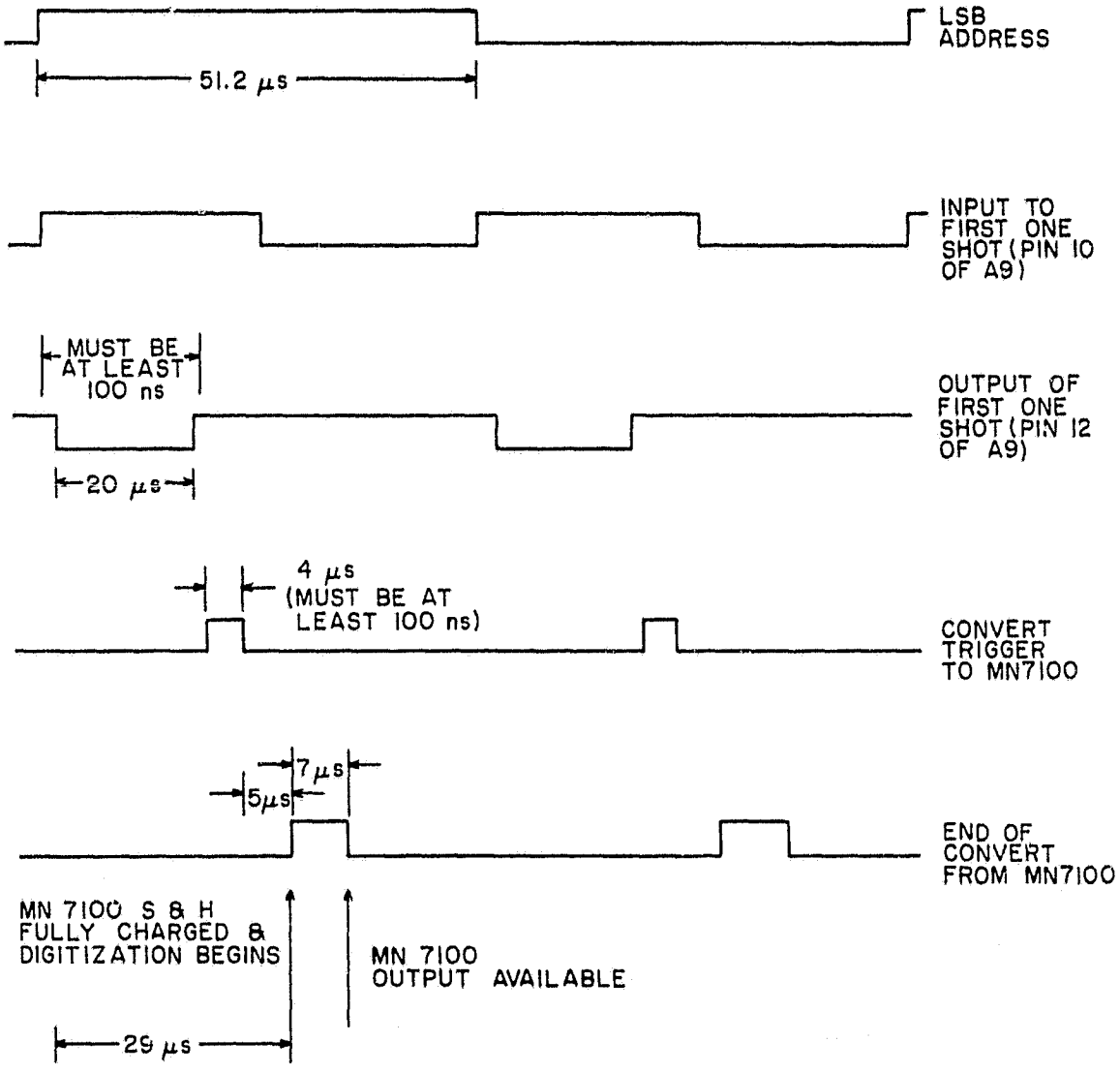

Figure 4.3 Timing diagram of the MN7100.

Although each peak detector is connected to two MN7100 inputs, only channels 0 through 3 are read. The jumpers connecting the other inputs could have been left off and inputs 4 through 7 grounded.

4.3 *The Peak Detector Discharger*

Once the peak detector's voltage has been read by the MN7100 (as shown by the fall in the EOC line) the peak detector must be discharged so that it will be ready for the next sample period. To do this, a Datel MXD 409 analog multiplexer is connected to the peak detector and, at appropriate times, the given input is switched to the output of the MXD 409 and thus is connected to ground, discharging the capacitor. When switched on, the input is connected through a saturated MOSFET with an on resistance of less than 2 kΩ. The worst-case discharge time constant is, therefore, 9.4 μs. The MXD 409 pin diagram is shown in Figure 4.4.

The MXD 409 is controlled by the same two address lines as the MN7100 and also by an inhibit line. The inhibit comes from the discharger inhibit (A12). The discharger inhibit is an inclusive OR gate tied to two lines operating, respectively, at twice and four times the LSB address line. The result is shown in Figure 4.5. Specifically, the inhibit line is high during the first 75% of each state of the LSB address. Therefore, the peak detector starts the discharge 38.4 μs after any change in the LSB address. This is 9.4 μs after the MN7100 is through reading the detector and has started to digitize the results. Since the discharge time is 12.8 μs or only 1.36 times the worst-case time constant, 26.6% of the previous value could remain after the discharge.

4.4 *Sampling Times*

Since the exact sampling characteristics are important for analysis of the data, the result of the operation of the circuitry discussed in the last two sections is now discussed in detail.

Consider the sampling from a single detector and refer to Figure 4.6. Assume that the discharger is completing the discharge of the peak detector for the detector of interest. The address lines to the MN7100 and the MXD 409 will simultaneously command both of them to move to the next channel and the discharger inhibit will inhibit the discharger.

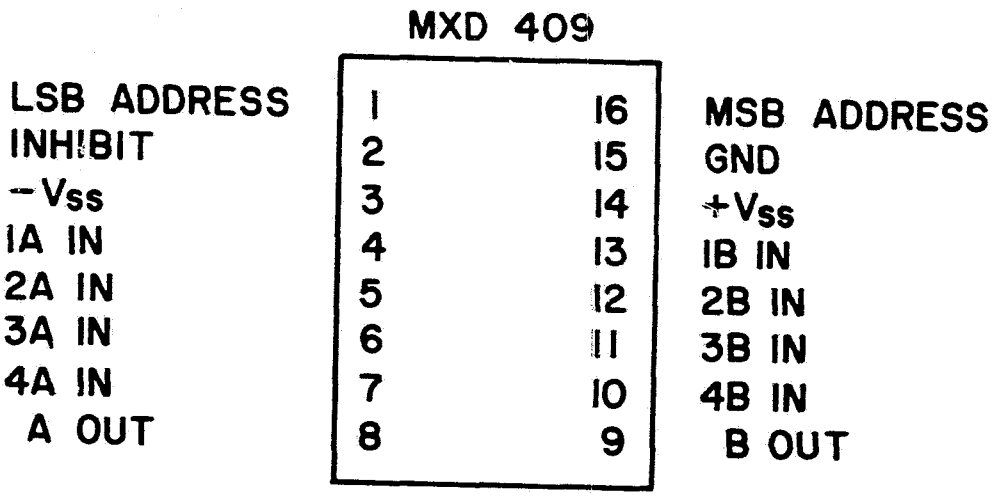

Figure 4.4 Pin connections for the MXD409 multiplexer. This is used to discharge the peak detector.

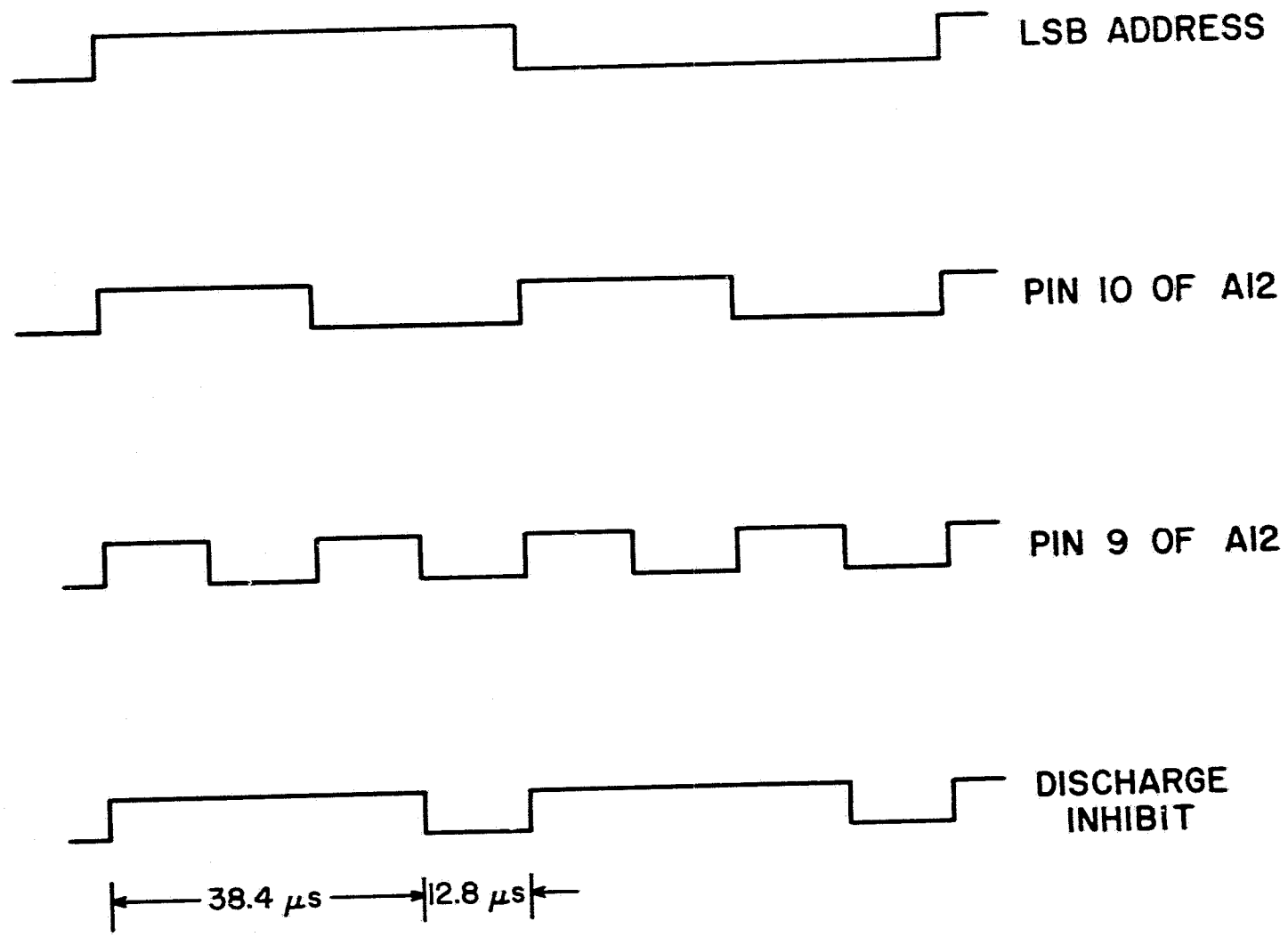

Figure 4.5 Timing diagram for the discharge of the peak detector.

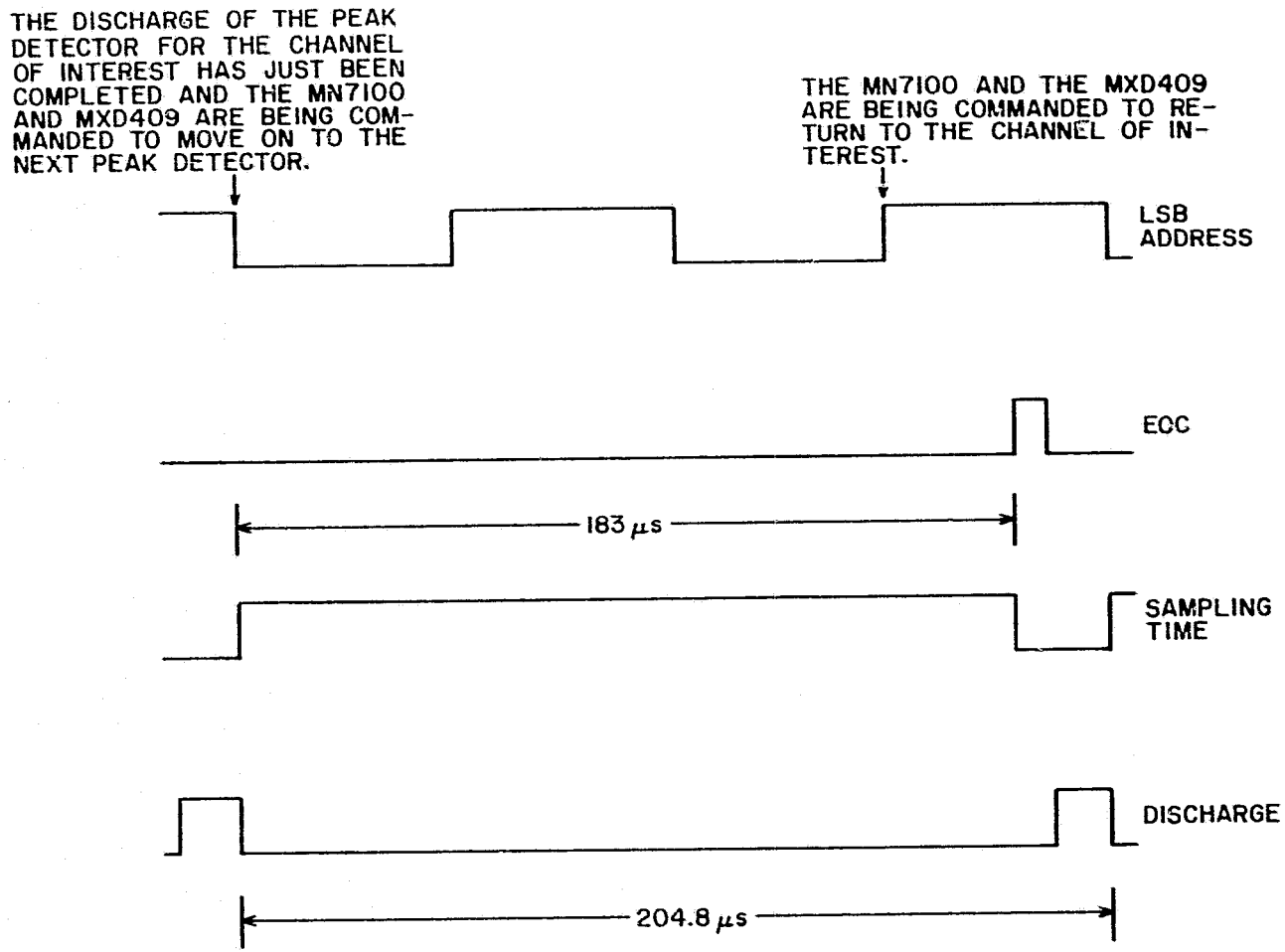

Figure 4.6 A summary of the sampling and discharge times for one channel over a complete operating cycle. The EOC, sampling time, and discharge time for the other three channels are delayed by multiples of 51.2 μs relative to the channel shown.

During the next 153.6 μs the MN7100 and the MSD 409 will be operating on the other three channels. After that, during the following 29 μs, the MN7100 will return to the channel of interest and charge up its sample-and-hold circuitry to the voltage on the peak detector. This voltage will, in turn, be proportional to the energy of the most energetic particle sampled during the 183 μs interval between the end of the last discharge of the channel of interest and the beginning of the digitization of the sample by the MN7100. The peak detector will continue to charge to any new energetic particle level sampled during the next approximately 9.4 μs, but the MN7100 will ignore this value. Then, during the last 12.8 μs before the LSB address line changes, the peak detector will be discharged.

Note that since the LM 318 in the peak detector has an output impedance of about 1 Ω (with the added output resistor) and the discharger has an impedance of 2 kΩ, pulses sampled during the discharge interval will be seen on the MN7100 input. However, they will not be read and their discharge will begin immediately.

4.5 *The Binary Dividers*

The control pulses discussed so far in this chapter come from a set of binary dividers. The binary dividers are made by cascading four synchronous dividers in a ripple-counter configuration. The counters as a whole are ripple counters so the transition times are not identical. However, the three most significant of the four divider lines discussed so far in the chapter come from one of the four bit synchronous counters in this chain. Therefore, the transitions discussed so far are approximately synchronous with each other.

4.6 *The MN7100 Output*

As part of the calibration procedure the gain of the circuitry preceding the MN7100 is set so that, if the system were perfectly linear, a 128 keV particle would cause a -10.0 V input to the MN7100. The MN7100 has 129 output levels corresponding to inputs from 0 to -10 V so that the output of the MN7100 is the two's complement of the negative of the energy (in keV) of the particle. A 45 keV particle, for example, causes a (45/128)(-10 V) = -3.52 V input to the MN7100. The magnitude of this voltage is simply 45 times 78.125 mV. The output of the MN7100 would be the two's complement of -45. The eight-bit signed digital representation for -45 is 1010 1101 and the two's complement

of this number is 0101 0011 or 53 in hexadecimal notation. 53 is, then, the output of the MN7100 corresponding to a 45 keV input particle.

Table 4.1 shows the output of the MN7100 for various energetic particle levels. If an input more negative than -10 V is applied to the MN7100, the MN7100 will put out the code for -10 V input.

4.7 *The Logarithmic Converter*

The logarithmic converter takes the digital outputs from the MN7100 and groups them into logarithmic intervals. The advantages of doing this were discussed in 2.5.3.

The logarithmic converter is an Erasable Programmable Read Only Memory (EPROM). An eight-digit output of the MN7100 is fed to the memory's address lines. The memory then reads out the contents of its memory at the address on its input. The program loaded into the memory is shown in Table 4.2.

To continue the example of the last section, the MN7100 would put out 53 due to a 45 keV particle. The logarithmic converter would, therefore, look up the contents of its memory at address 53. Referring to Table 4.3, 53 is in the range of 4D to 53 and the contents of the four most significant bits in memory at any memory address between 4D and 53 is 8. The logarithmic converter will then put out 8.

The EPROM was programmed so that the four most significant bits and the four least significant bits are the same at any memory address. However, only the four most significant bits are fed to the next stage, so the content of the four least significant bits is unimportant.

Table 4.3 shows the energy ranges and bins that would result if the system were perfectly linear. The result is slightly modified by the non-linearities of the system and is established by calibration.

4.8 *The FIFO*

The microprocessor system of *Davis et al.* [1979] and an early version of the one of *Braswell and Smith* [1981] were not able to accept data at all times. Most of the time when these microprocessors were unable to accept data was when they were on interrupt. In order to prevent the loss of data collected when the microprocessors were unable to accept data, all of the data from the PHA were temporarily stored in a first-in-first-out (FIFO)

Table 4.1

The MN7100 output corresponding to various energetic particle levels sampled.

Energy Level into Detectors (keV)	DC Input to MN7100 (Number of +78.125 mV Intervals)	Eight-Bit Signed Digit Representation of MN7100 Input		MN7100 Output (Two's Complement)		
				Digital		Hex
0	0	1000	0000	1000	0000	80
1	-1	1000	0001	0111	1111	7F
14	-14	1000	1110	0111	0010	72
16	-16	1001	0000	0111	0000	70
126	-126	1111	1110	0000	0010	02
127	-127	1111	1111	0000	0001	01
128	-128	0000	0000	0000	0000	00

Table 4.2

The logarithmic-converter program.

Addresses	First Four Bits of Memory Contents
000	F
001 - 012	E
013 - 022	D
023 - 02F	C
030 - 03A	B
03B - 044	A
045 - 04C	9
04D - 053	8
054 - 059	7
05A - 05E	6
05F - 063	5
064 - 067	4
068 - 06B	3
06C - 06E	2
06F - 071	1
072 - 7FF	0

Table 4.3

The logarithmic-converter output related to particle energy with a perfectly linear system.

Particle Energy Level (keV)	MN7100 Output (Hex)	EPROM Output
0 - 14	80 - 72	0
15 - 17	71 - 6F	1
18 - 20	6E - 6C	2
21 - 24	6B - 68	3
25 - 28	67 - 64	4
29 - 33	63 - 5F	5
34 - 38	5E - 5A	6
39 - 44	59 - 54	7
45 - 51	53 - 4D	8
52 - 59	4C - 45	9
60 - 69	44 - 3B	A
70 - 80	3A - 30	B
81 - 93	2F - 23	C
94 - 109	22 - 13	D
110 - 127	12 - 01	E
≥ 128	00	F

memory. Then, when the microprocessor was able to accept data, it commanded the FIFO to read out its data. The FIFO was also used to append to the data sampled sector identification and a bit supplied from the microprocessor and referred to as memory select.

The final microprocessor system of *Braswell and Smith* [1981] incorporates a peripheral interface adapter (PIA) and is, therefore, able to accept data at any time. The memory select line is also unnecessary with the current microprocessor. Therefore, the memory select and the advance FIFO input lines are connected high in the microprocessor and the FIFO reads out data shortly after it is received from the logarithmic converter regardless of microprocessor functioning. The FIFO was retained in these flights due to time limitations. Elimination of the FIFO circuitry is recommended in future flights.

It requires 450 ns for the logarithmic converter to operate. The end-of-convert (EOC) line from the MN7100 is applied to the input of one of the one shots in A11. The one shot puts out a 700 ns pulse on pin 5 which goes to the FIFO's shift in. The falling edge of the output of A12 locks the input registers in the FIFO to the logarithmic converter's output.

When the FIFO is loaded and ready to put out data, it puts a high on its output ready line (pin 12). The output ready line is fed, along with the advance FIFO in line (always tied high) and a binary divider line output with a pulse width of 1.6 μs to inputs of a 3 input NAND gate in A10. The NAND gate provides a means of triggering the second one shot in A11. The first rising edge of the NAND gate triggers the data ready out pulse out of A11 which shifts the data out of the FIFO and tells the microprocessor that the current PHA card output is valid.

The data lines out of the PHA have the significance shown in Table 4.4.

Table 4.4

PHA output lines

Data Ready Out	Indicates that the current output is valid	
I_0	LSB	Data
I_1		
I_2		
I_3	MSB	
I_4	LSB Address	
I_5	MSB Address	
I_6	Memory Select	
I_7	No Meaning	

5. SYSTEM INTEGRATION

The equipment described in this report is included in payloads built for Taurus Orion rockets. Three were flown in November 1980 during the Energy Budget Campaign. The configuration of the payloads is shown in Figure 5.1. The diameter of the instrumentation section is 30 cm. At the front is an ejectable nose cone, protecting the input section of a mass spectrometer (University of Bern). Ejection takes place at an altitude of T + 52 s (57 km, nominal altitude) and the cap of the mass spectrometer is ejected 2 s later (at 60 km).

Doors in the rear experiment section are also ejected at T + 52 s (57 km) and booms deployed at T + 60 s (67 km). The booms carry the electrodes of the probe experiment and the forward-looking energetic-particle detectors. The spin rate at boom deployment (and for the scientifically significant part of the flight) was specified to be 5.5 rps. The actual values (at apogee) for the three payloads range from 5.86 and 5.98 rps. The rockets showed very little precessional motion.

The portion of the payload containing the experiments of the University of Illinois is shown in Figure 5.2. A particle-bunching experiment (University of Sussex) is also included in this section of the payload.

One particle detector for the EPS system is mounted on each of the two booms. After the booms are deployed, the detectors on the booms are aimed at a 25 degree angle with respect to the spin axis of the payload. These detectors are identified as EPS channels one and two.

The other two detectors are mounted on the deck marked "particle detectors, pulse-height analyzer, and counting circuits" in Figure 5.2. They are adjacent to each other and are both aimed in the same direction. That direction is 90 degrees with respect to the payload spin axis. These detectors are identified as channels three and four.

The geometrical factor (GF) for the forward-looking detectors is 0.45 cm^2ster; the large value was chosen to give a high count rate for the particle-bunching experiment. The full width at half maximum (FWHM) is 59 degrees. The side-looking detectors have GF = 0.057 cm^2ster and FWHM - 18 degrees. The narrower field of view is chosen to give better pitch-angle resolution.

One of each pair of detectors has an increased thickness of aluminum on

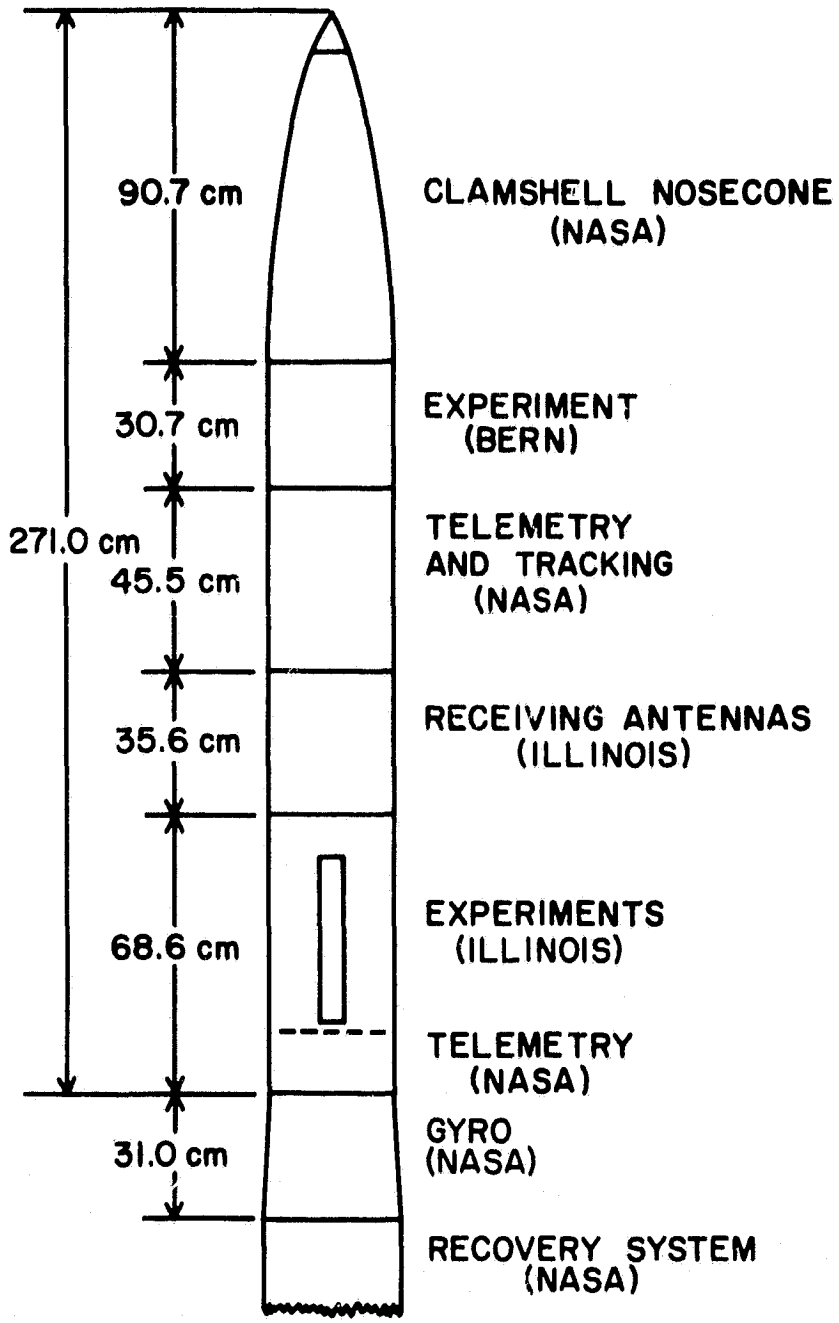

Figure 5.1 The payload, flown on Taurus Orion rockets during the Energy Budget Campaign.

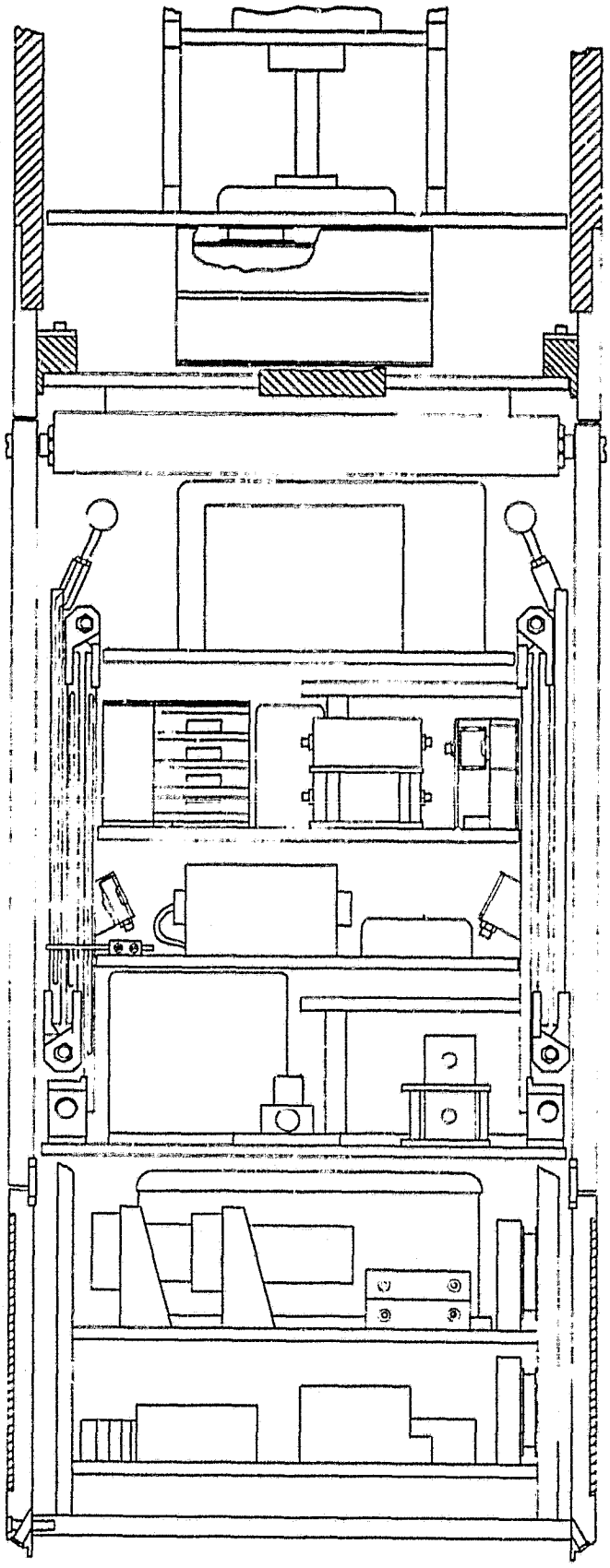

Figure 5.2 The portion of the payload containing experiment of the University of Sussex and the University of Illinois.

the front surface. The comparison of the flux seen by the pair of detectors allows some discrimination regarding the type of energetic particle (electron, proton, etc.). This technique has been described by *Fries et al.* [1979]. The specifications of the detectors are summarized in Table 5.1. The preamplifiers for all four detectors are mounted on the shelf containing detectors three and four. Since the coax cables between detectors three and four and their respective preamplifiers are much shorter than those for detectors one and two, channels three and four have a much lower noise level. The shapers are also mounted on the same shelf as the preamplifiers.

The staircase-generator card, the PHA card, and the card containing the amplifier and threshold detectors for the bunching experiment plug in to the EPS card cage. The EPS card cage is shown mechanically in Figure 5.3 and schematically in Figure 5.4. The EPS card cage and a similar card cage for the microprocessor (also shown in Figure 5.3) allow versatile development. The two card cages were designed so that they may be plugged together (as shown in Figure 5.3) so that they could also be used in payloads of 6.5 in (16.5 cm) diameter.

Table 5.1

Energetic particle detectors.

NUMBER	METAL ($\mu g/cm^2$)	ANGLE (deg)	GF ($cm^2 ster$)
1	40 Au + 40 Al	25	0.45
2	40 Au + 150 Al	25	0.45
3	40 Au + 40 Al	90	0.057
4	40 Au + 150 Al	90	0.057

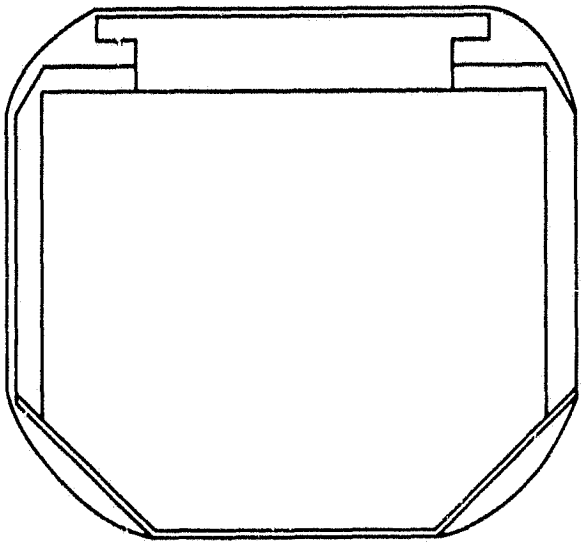

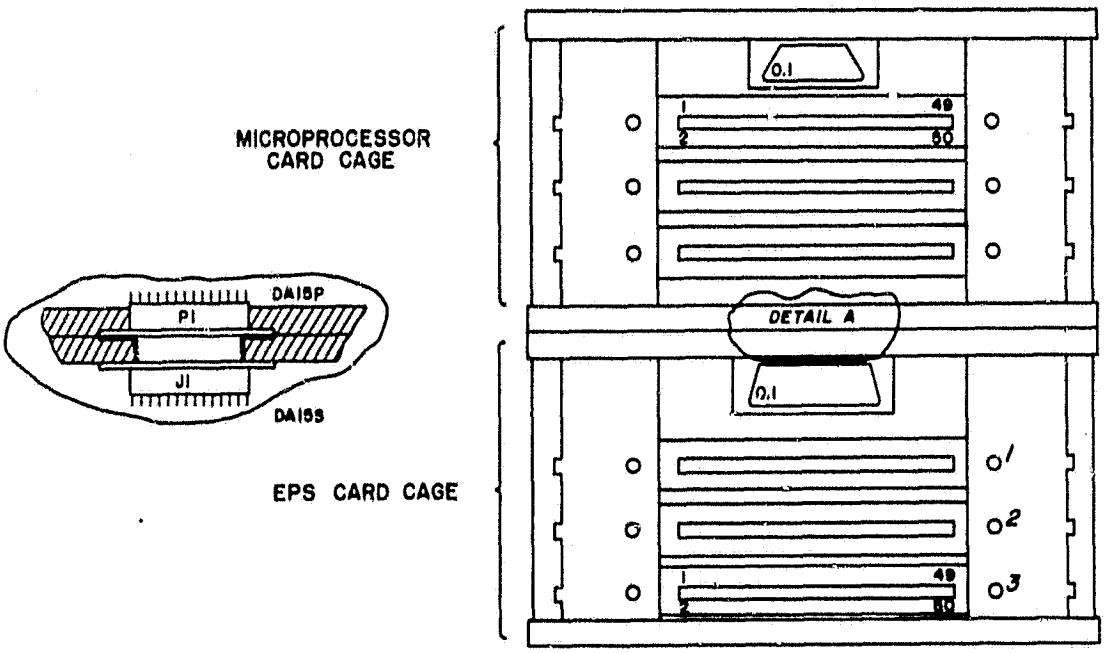

1 AMPLIFIER & THRESHOLD DETECTORS OF BUNCHING EXPERIMENT

2 PULSE HEIGHT ANALYZER CARD

3 STAIRCASE GENERATOR CARD

Figure 5.3 The card cages used for the energetic particle experiment. The two cages may be used separately or plugged together.

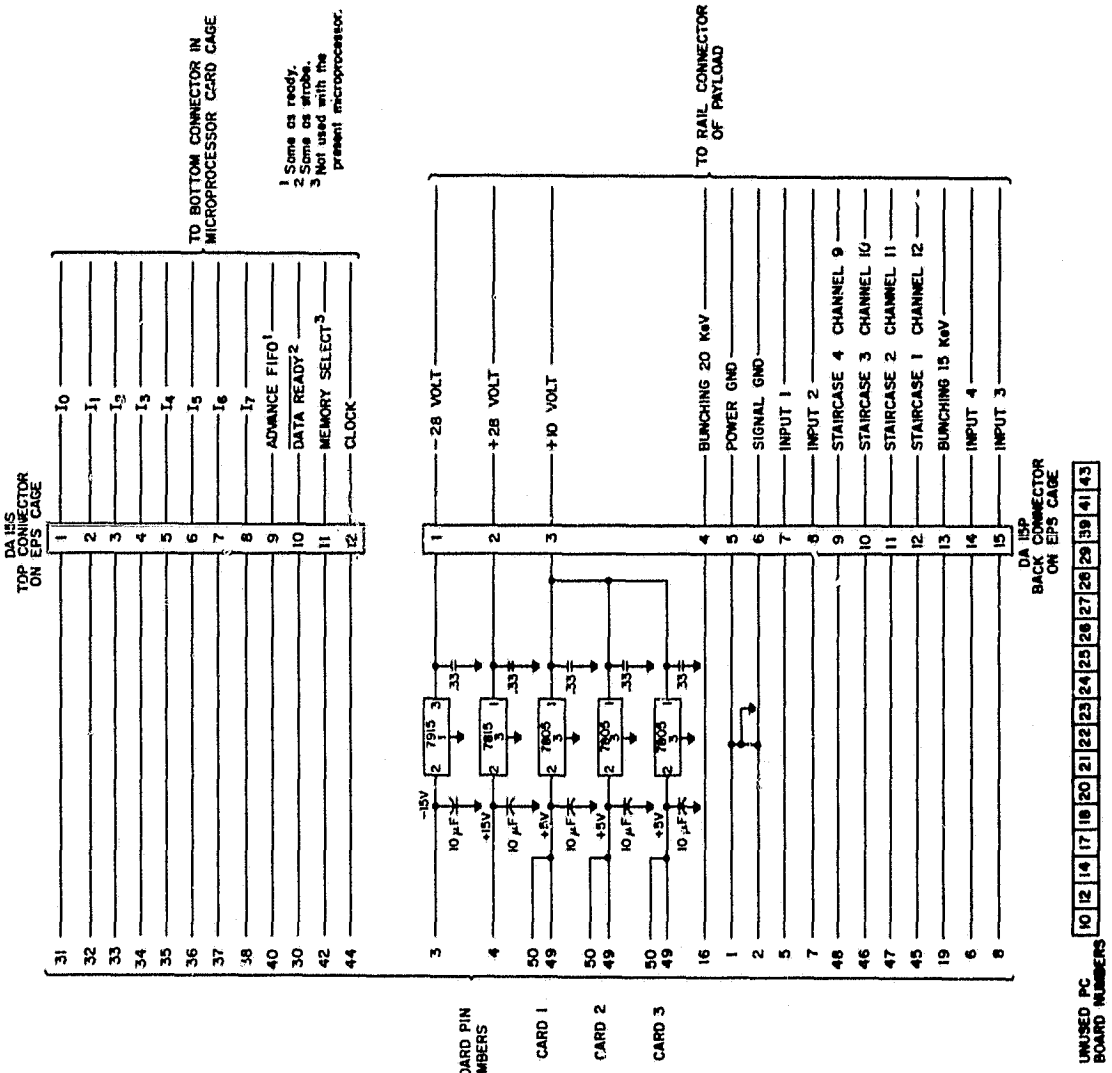

Figure 5.4 Circuit diagram for the EPS card cage.

6. CALIBRATION

Calibration of the EPS system involves setting the gain of each of the four amplifiers on the staircase-generator card, making calibration curves, and setting the proper reference voltage for the comparators on the staircase-generator card.

6.1 *Setting the Gain*

Since the entire EPS system is made with fixed parts, the gain of each part of the analog portion of the system varies from unit to unit. The gain of the amplifiers on the staircase-generator card are adjusted so that the total gains from the detectors through the peak detectors are correct.

The desired range of particle energy to be measured on these flights is 0 to 128 keV. Since the MN7100 has 129 output steps for the range of 0 to -10 V input (see Table 4.1), -10 V out of the peak detector is desired for a 128 keV particle. Consequently, a (60/128)(-10 V) = -4.69 V pulse out of the peak detector would be required for a 60 keV energetic particle.

A 1 μC radioactive source of Am 241, which has a strong emission at 60 keV, is used as the standard to calibrate the system. Two precautions must be noted at this point. First, the radioactive source must be used with caution. It must be stored in a lead box and it must be handled with pliers. Second, a new source should be used to prevent serious calibration errors. The source puts out energies other than 60 keV and this can lead to errors. While new and old sources put out the same energy levels, the predominant high energy output of a new source is at 60 keV while the 60 keV output count rate will be less than some of the other outputs if an old source is used. Therefore, the notion that an old source is preferable since it is not so dangerous to handle, may lead one to gross errors in system calibration. To prevent this ambiguity with the source, one should use a source well within the half life stated by the manufacturer of the source. Plastic should be placed over the source to block alpha particles.

The source should be placed near, but not in contact with, one of the detectors and the output of the corresponding peak detector monitored on an oscilloscope. The oscilloscope's vertical channel should have a risetime of 100 ns or less. A storage oscilloscope makes the calibration easier. The discharger may be unplugged so that the peak detector output is more easily

observable. The predominant output voltage of the peak detector due to the particles should be noted and the gain of the first amplifier on the staircase-generator card adjusted until this level is -4.69 V. When the gain is approximately correct, the oscilloscope's vertical gain should be increased and the peak detector output voltage compared with a precision dc voltage source. Once the gain of the amplifier is set, the radioactive source should be removed and an Ortec 448 (or similar) pulse generator connected as shown in Figure 6.1. The variable attenuator (the large concentric knobs on the Ortec 448) should be set to 06000, to correspond to 60.00 keV, and the toggle switch attenuators adjusted for a -4.69 V pulse out of the peak detector. A calibration curve may then be obtained by leaving the toggle switch attenuators alone and changing the variable attenuator while recording the corresponding peak detector output voltage. The result is a calibration curve such as in Figure 6.2. The above calibration procedure is done for each of the four detectors, one at a time.

The calibration curves track each other very closely except for the non-linear region at high energy levels. The non-linearity is due to limiting by the LM318 in the peak detector. This is not a serious problem but may be avoided in future flights by increasing the dc supply voltage for the LM318's. Due to the non-linearity, the actual range of the highest 3 bins for the detector shown in Figure 6.2 are: D, 93 to 116 keV; E, 117 to 200 keV; and F, > 200 keV.

6.2 *Alternate Method of Setting the Gain*

The gain may also be adjusted by looking at the output of a test box connected to the microprocessor output. A schematic of the test box is shown in Figure V.4 of *Braswell and Smith* [1981]. The output of the microprocessor is a serial digital code. The test box converts the serial digital code into a parallel digital code and then supplies the parallel code to a D/A converter.

The output of the D/A converter is shown in Figure 6.3 for an Am 241 source and low flux. The oscilloscope is connected to display the D/A output voltage and is set to trigger on the large marker pulse shown at the left of the picture. There are 15 intervals shown between the marker pulses. The intervals, starting with bin one, correspond to the 15 significant energetic particle energy range bins from the logarithmic converter. The

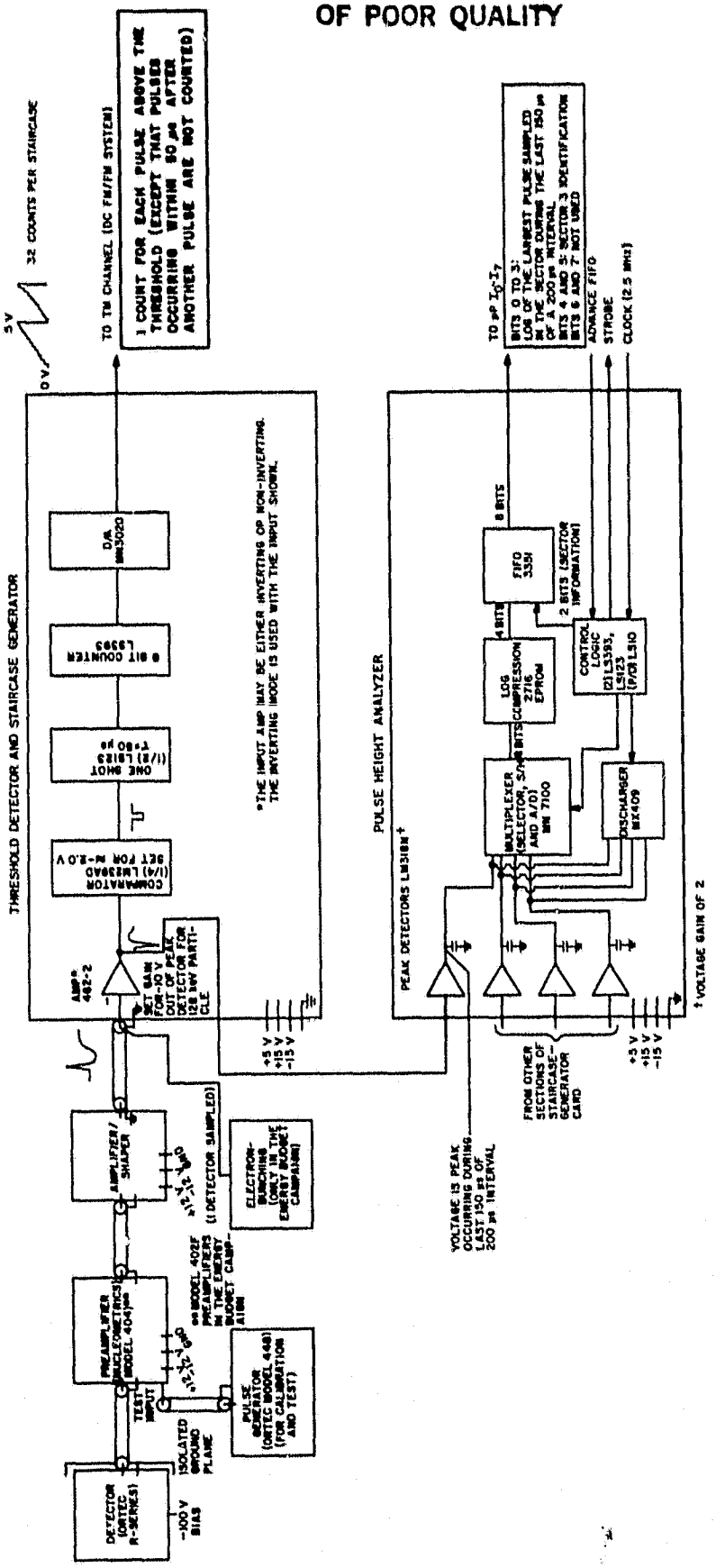

Figure 6.1 The configuration of the experiment for calibration.

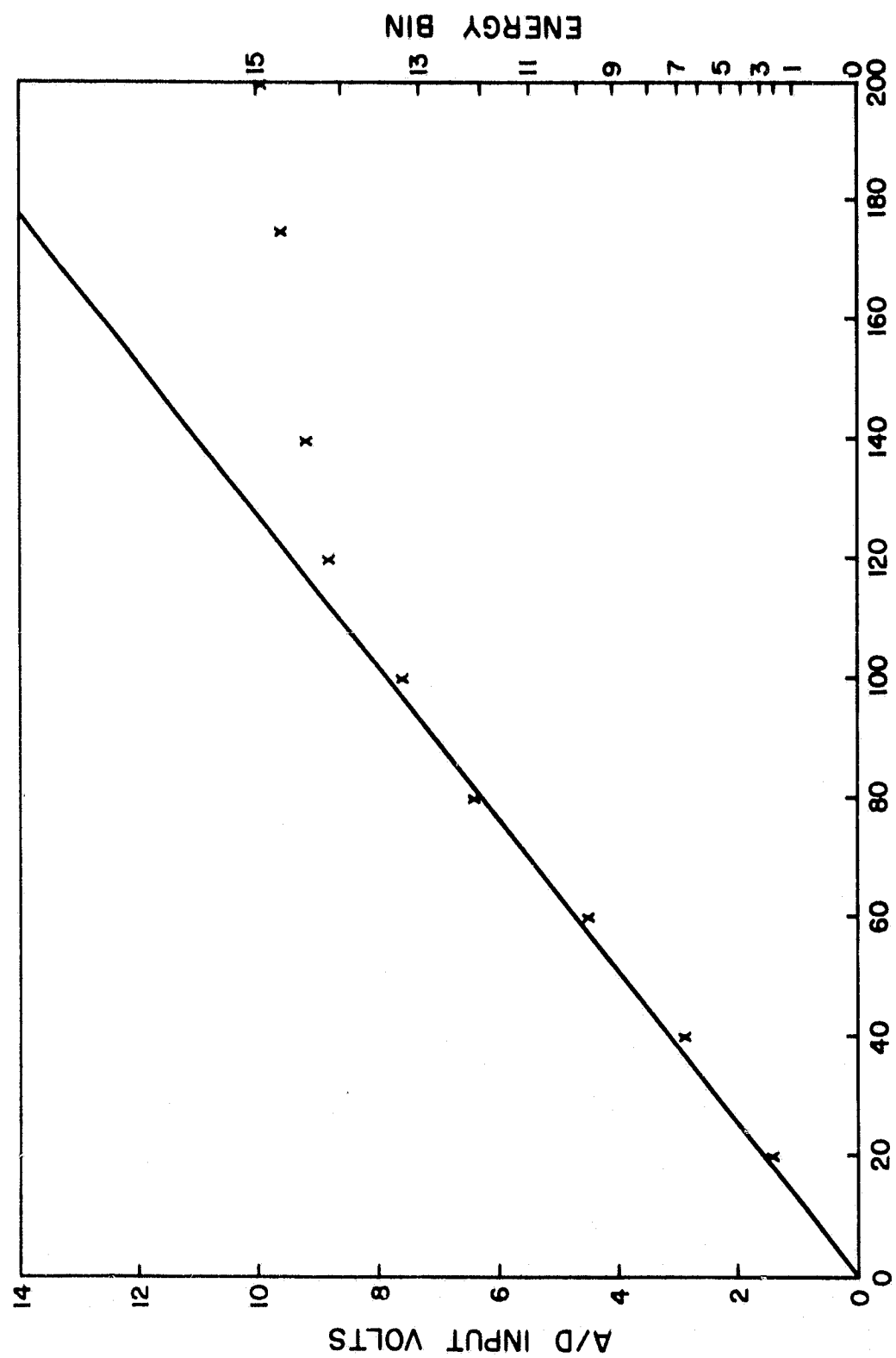

Figure 6.2 Calibration curve for the energetic particle spectrometer [*Braswell and Smith*, 1981].

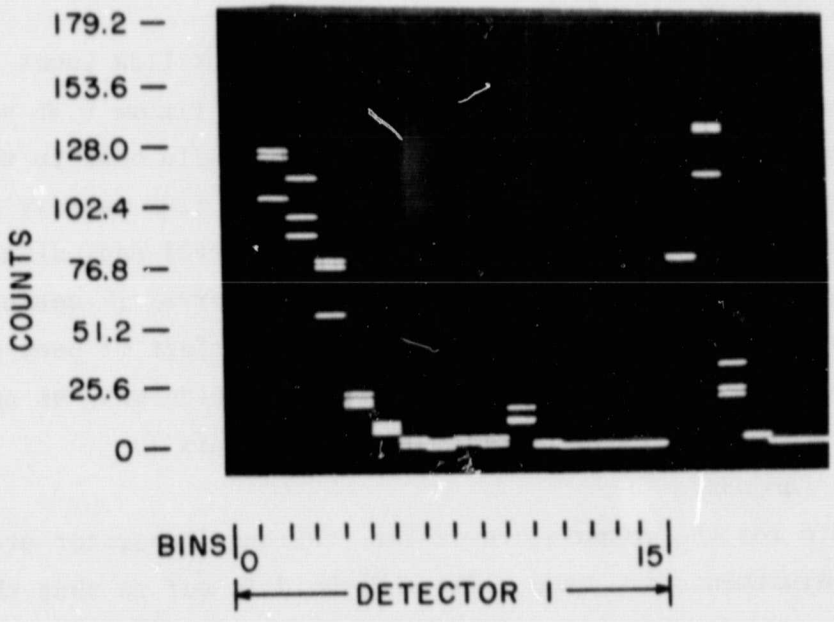

Figure 6.3 An alternate calibration method is to adjust the gain until the 60 keV line of Am 241 appears in bin 10 [*Braswell and Smith*, 1981].

scope's vertical input is linearly proportional to the number of counts received in the bin, provided that the microprocessor's bin has not overflowed. In the photographs of Figures 6.3 and 6.4, the camera shutter was left open for many system cycles, so several different counts are present for some of the bins.

The proper amplifier gain may be obtained by adjusting the gain resistor until the predominant output with an Am 241 source falls in bin 10. This approach makes the calibration a simple process, but is less accurate than the method of section 6.1.

6.3 *The Effects of Peak Detection*

Figure 6.4a, which was taken with a low energy flux (low count rate), shows the true energy distribution from a Ni source. Figure 6.4b shows the output due to the same source when that source is held next to the detector so that a very high flux exists. With a high flux, a very energetic particle was received in almost every data sample interval and, since with peak detection only the largest sample in a sample interval is measured, virtually no low energy particles are measured. The effect of peak detection with high flux is illustrated in Figure 6.5. A correction must be applied to the data in such cases. This is discussed in Appendix I.

6.4 *Setting the Threshold*

The threshold for the comparators of the staircase generator are set *after* the gain adjustments are made. The threshold is set so that the comparator will not trigger on noise. In the past, as discussed in Section 2.5.1, four threshold amplitude detectors were connected to the output of each of the amplifiers and each of the threshold detectors was followed by circuitry that generated a staircase. This required four TM channels for every detector being sampled. With the greater data amplitude information now available from the remainder of the EPS system, the twelve TM channels that are saved by going to a single threshold for each of the four detectors are being better utilized by other experiments. This change to a single threshold has raised the question of what that threshold should be. Previously, the lowest threshold level was set right at the noise level so that it would count occasional noise peaks. This gave persons at the launch site confidence that the experiment was working while leaving three threshold levels for "real" counts.

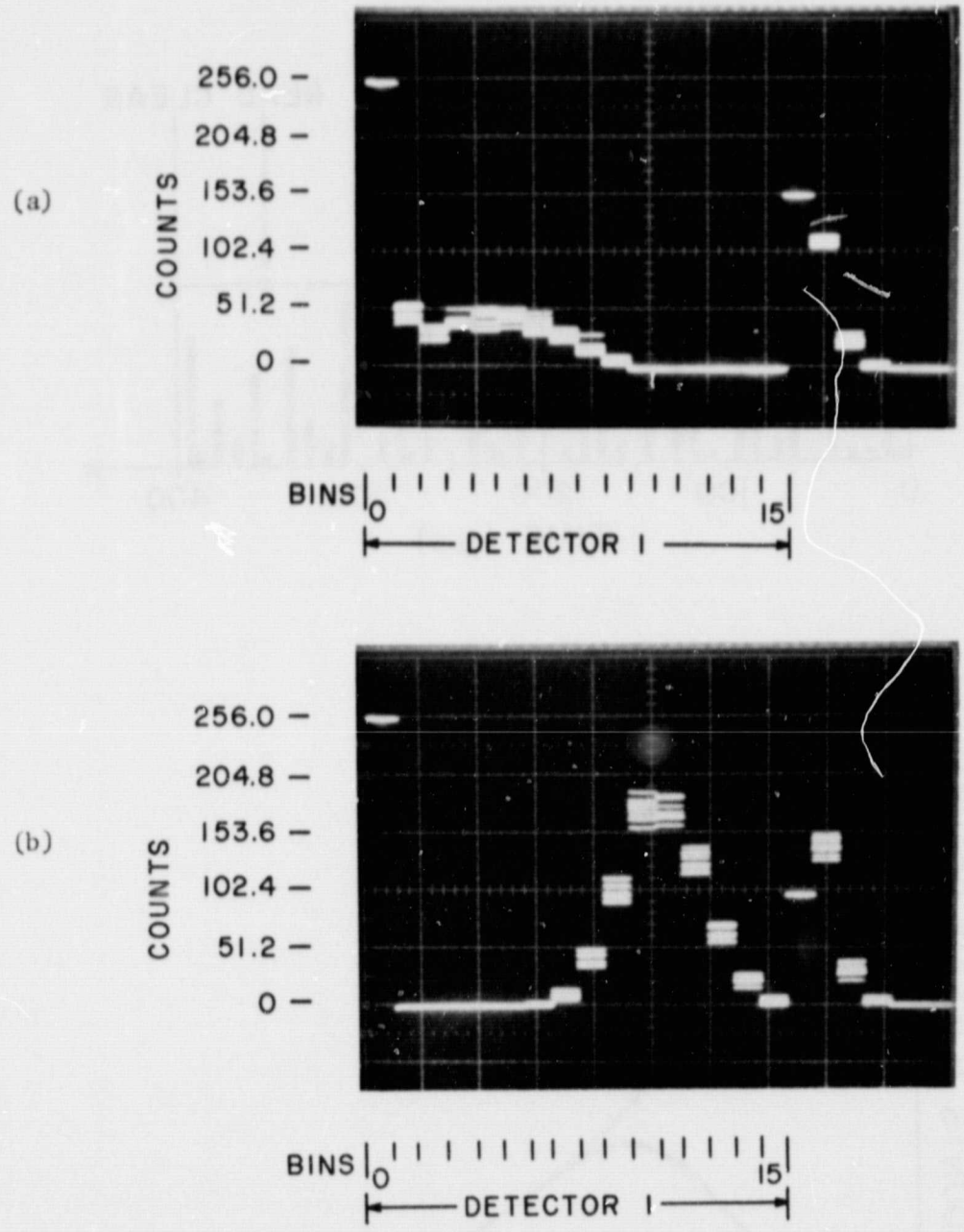

Figure 6.4 The distortion in the observed energy spectra with a high flux due to sampling error in the peak detector. (a) A Ni source is held far enough from the detector so that a low flux exists and the spectrum is accurately displayed. (b) The same source is held next to the detector resulting in a distorted spectrum [*Braswell and Smith*, 1981].

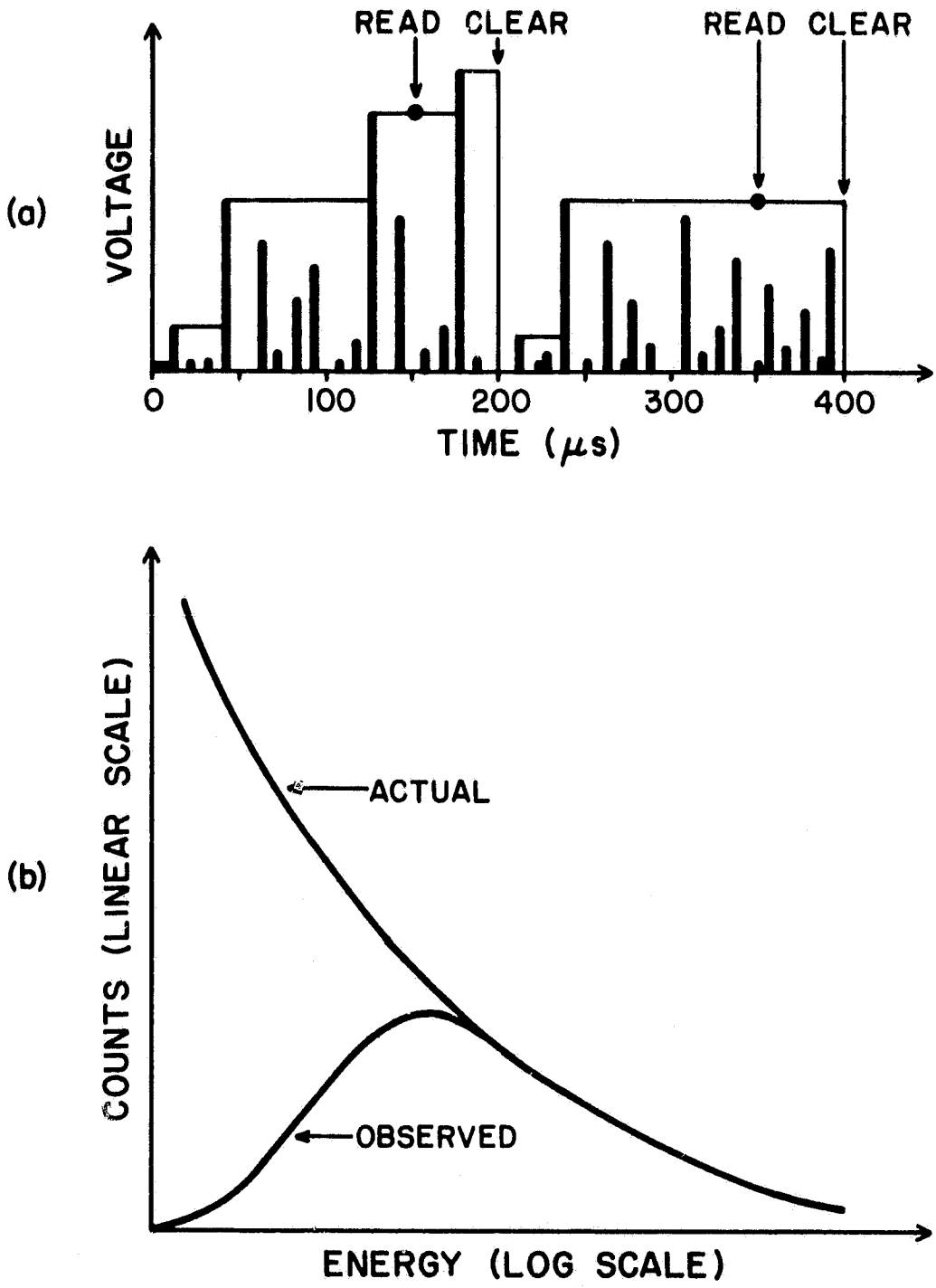

Figure 6.5 Sampling error in the peak detector distorts the energy spectrum at high particle fluxes.

Initially, the (single) threshold was set just above the noise, but the system noise level changes by about 1 dB with ambient temperature, the length of time since turn-on, and the amount of time the system has been powered up recently (the last two items probably primarily affect detector impurities). Therefore, the threshold level is now set to about 1.5 dB above the noise. Note that this setting does not affect amplitude measurements by the pulse-height analyzer.

The threshold for a given staircase generator is set by first replacing the lower resistor in the voltage divider to the appropriate comparator section with a resistor decade box. The value is adjusted until that staircase generator counts (randomly) about one count every five seconds and the value of the resistor is noted. Since the lower resistor's value is much less than a tenth of the upper resistor value, for small changes in the lower resistor, the voltage reference is roughly proportional to the lower resistor. Therefore a threshold increase of approximately 1.5 dB can be obtained by multiplying the lower resistor by $20^{0.15} = 1.6$ and selecting the next higher standard resistor value. This procedure is repeated for each comparator.

7. RECOMMENDATIONS FOR FUTURE WORK

The circuitry developed on the project gave useful data on the peak energetic particle levels. However, as discussed in Section 6.3, due to the use of peak detection in a high count rate environment, the measured distribution of the energy amplitude is distorted. Furthermore, the determination of the actual distribution is difficult. This chapter will primarily focus on how the circuitry can be modified to prevent this problem in future flights. Some other modifications which improve the performance of the equipment are also suggested. It can be noted that, in most flights done in the past at middle and low latitudes, the count rates have been low enough that the distortion in the energy distribution has been negligible.

7.1 *Basic Alternatives to Improve Sampling Statistics*

The first alternative to come to mind is to leave the circuitry basically as it is, but to run it at a much faster speed. Certainly if the time interval for charging the peak detector was made smaller, a given count rate would be less likely to cause two or more counts to occur during the interval. Of course, the probability of one count also decreases, so the improvement is not as great as the decrease in the probability of two or more counts suggests. The reduction in the distortion of energy distribution is determined by the ratio of the two probabilities. In order to make a significant improvement in the energy distribution under the conditions observed in Sweden, the speed of the system would have to be at least doubled and this would cause several new problems to develop. First, the radio channel bandwidth and the microprocessor speed would both have to be increased unless the PHA was modified so that it only had a low duty cycle or only a small sample of its data was supplied to the microprocessor. This could affect NASA ground equipment as well as requiring a major rocket payload redesign. In addition, if the PHA had a low duty cycle, the low sample obtained in the event of a low flux density (low count rate) would cause very poor data statistics. Furthermore, as the peak detector charge time is reduced, the probability that a measurement would be made on the rising edge of the shaper's output, rather than on its peak output, increases dramatically. Finally, if the speed of the PHA were substantially increased, the timing

would become very critical. The one shots used in the PHA for timing would be unacceptable. The result is that the PHA control circuitry would become much more complicated. For these reasons, increasing the speed is not recommended.

A second solution would be to decrease the count rate by decreasing the geometrical factor of the detectors. The GF could be varied in accordance with the projected count rate. This is a simple solution, but to be effective, the projection of the flux density should be fairly accurate. An error in the projection could either cause excessive count rates (so that the problem would not have been solved) or inadequate count rates which would lead to poor statistics. Furthermore, since the count rates typically vary widely in a flight as a function of the altitude and the rocket spin angle the resulting data would be unacceptable during at least part of a flight. For these reasons reducing the GF is not recommended.

The optimum solution is to measure the first, and only the first, pulse to occur during a sampling period. This solution would give an accurate energy distribution and would be self-adapting in the sense that it would work over a large range of count rates. The solution, as discussed below in Section 7.3, would not require microprocessor or other system modifications.

The sample statistics would also be improved if the discharger time constant were shorter so that the peak detector was essentially fully discharged. In *Leung et al.* [1979] the peak detector is discharged by being connected to a voltage of the opposite polarity, rather than to ground, to improve the discharger's operation. However this change is not a solution since the amplifier of the peak detector has a low output impedance and still charges the capacitor of the peak detector if a pulse is received during the discharge time. The circuitry of Section 7.3 eliminates this problem.

7.2 *Other Changes*

To improve system performance, the first amplifier on the staircase-generator card should be returned to the shaper card. This would reduce the effective noise level by eliminating the extraneous signal pick up before the amplifier. Of course, the same amount of extraneous signal would be picked up, but the desired signal would be increased by the gain of the

amplifier before the pick-up point (the cable between the shaper and the staircase-generator card), so the signal-to-noise would be improved. The amplifier should retain its present capability to be used in either the inverting or the non-inverting mode, but in any given system it should be connected to give a positive pulse out to work with the remaining circuitry to be suggested in Section 7.3. The amplifier should be replaced by an LM318 for cost reduction. Since the space on the shaper where *Fries et al.* [1979] had the amplifier is now unused, the required modification is minimal.

The nonlinearity can be eliminated by adding ±18 V regulators to supply power for the LM318's in the peak detectors. If it is desired to accurately measure energetic particles of greater than 128 keV, the gain of the amplifier moved to the shaper could be reduced and the logarithmic converter re-programmed. If the gain were halved, the range would be doubled to 256 keV but the resolution would also be halved. Relying on the nonlinearity of the peak detector for high energy measurements is not recommended as the nonlinear characteristic is probably not consistently repeatable.

The important pulses from the binary dividers should be made synchronous with each other by deriving all of them from one of the synchronous four bit binary dividers. The next section shows how this can be done without increasing the number of chips required.

The FIFO is now only used to append the sector information; it should be eliminated for greater reliability and to make room for the added circuits of the next section.

Since the bunching experiment will not be included in future flights, the room occupied by that circuit can be used for the circuits discussed in the next section.

The recommended circuit uses interconnected TTL gates on different cards. Therefore, the card cage's multiple +5 V regulators should be replaced by one regulator (such as the LM309) capable of supplying the entire cage's +5 V.

The shaper would now put out a positive pulse, so that the references for the comparators in the staircase generator card would be changed to positive voltages. This only requires replacing one wire. The one shots should then be changed to trigger on a rising (positive-going) edge. This can be accomplished by changing the inputs of the one shots from pins 1 and

9 to pins 2 and 10 respectively and grounding pins 1 and 9.

7.3 *The Recommended PHA Circuitry*

The recommended PHA configuration is shown in Figure 7.1. The first amplifier of the staircase generator card (not shown) would be moved to the shaper, as discussed earlier, and it would be configured so that its output pulse is positive. The staircase generator modifications of the last paragraph are also assumed, but not shown.

The noninverting mode for the first amplifier of the PHA would be retained as this configuration has a high input impedance so that an attenuator placed between the card input and the amplifier would be effective. That attenuator consists of the input resistor and the open collector of the hex inverter. When the inverter transistor is off, the 10 kΩ input resistor has little effect due to the very high input impedance of the amplifier and inverter transistor. However, when the inverter transistor is on the input signal is attenuated. By turning the inverter transistor on after the first pulse is sampled during a sample period, no further signal will reach the peak detector.

The input pulse and the peak detector output are both changed for positive pulses so that conventional TTL logic gates with open collectors may be tied directly to these points. The input diode prevents the negative overshoots from being seen by the TTL circuitry.

The output of the peak detector is sampled by a LM239 comparator. The threshold is set to correspond to the bottom end of the first logarithmic converter range (above the noise). Referring to Table 4.3, the first range above the noise currently starts at 15 keV. Therefore, the threshold should be (15 keV)(78.125 mV/keV) = 1.17 V. The comparator puts out a zero except whenever the dc input is greater than the threshold. When a particle is sampled, the input rises above the threshold and a discrete pull-up resistor applies a one to the one shot.

The one shot is set to trigger on a rising edge. It is set to about 2 μs to allow the peak detector to charge to the peak of the pulse (as stretched by the shaper). After allowing time for the peak detectors to fully charge, the one shot sets a SR flip flop which drives the inverter used in the attenuator. The signal voltages in the PHA would then remain constant

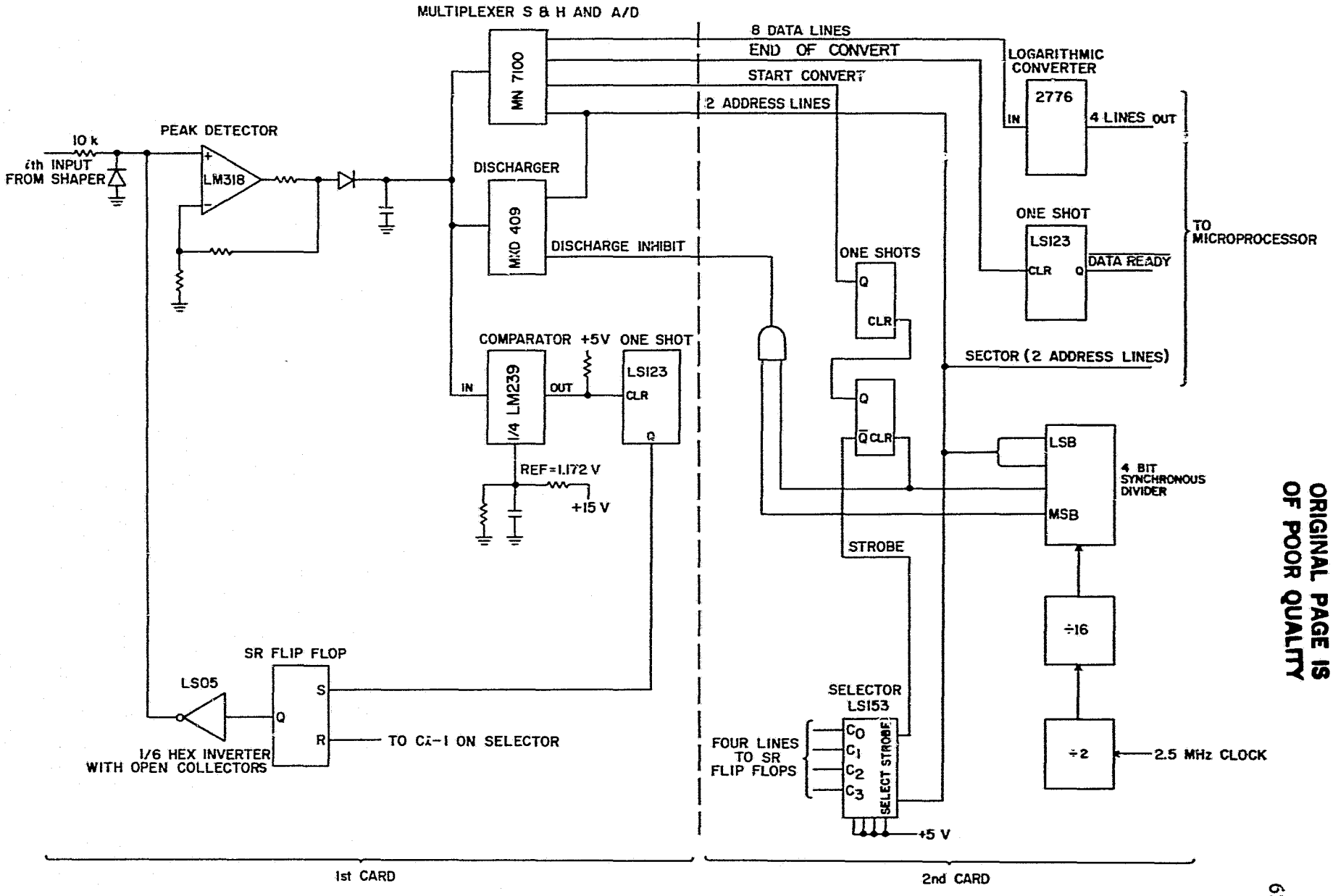

Figure 7.1 Recommended PHA configuration.

(even if new particles struck the detector) during the remainder of the sample window and then also while the control circuitry commands the MN7100 to read the peak detector output. The attenuator would remain on while the discharger charged the peak detector toward -15 V. This would ensure that the capacitor would be throughly discharged even if a particle struck the detector during the discharge time.

At the end of the discharge time, the control circuitry would command the MN7100 and the MXD409 to move to the next channel. The first one shot of A9 (which triggers when the LSB address line is changed) would have its time shortened to about 5 μs and its output would also be fed to a multiplexer such as the 74LS153. The multiplexer would be set up so that it would reset the flip flop of its address minus one. This would be accomplished by, for example, tieing the C2 output to the flip flop for detector 1. This would reset the flip flop and remove the attenuation so that the peak detector would recharge.

The logarithmic converter would be reprogrammed for positive input signals and the FIFO eliminated.

The new PHA circuitry would be distributed over two circuit cards as shown in Figure 7.1. This distribution would require the use of 17 additional lines between the EPS cards. Figure 5.4 shows that there are now 18 unused lines, so this is no problem. Three fewer lines would be required if the 74LS153 selector were moved to the other card, but this might unnecessarily crowd the other card.

Note that all of the lines used from the binary dividers come from one section of one of the 74LS393 4-bit synchronous binary counters. This ensures that all of the lines are synchronous with respect to each other.

The best way to demonstrate the effectiveness of the proposed circuit would be to note that the observed energy spectra would not change (as it does in Figures 6.3a and 6.3b) as the energy flux is varied. Furthermore, the circuitry should give good statistics in a low flux environment. It is believed that the circuitry discussed above would perform well in these tests.

7.4 *Further Refinements*

A problem in the alternate calibration method of Section 6.2 is that, for example, 60 keV is read out in bin A which is 10 keV wide. Therefore,

a potential alignment error of (9/60)(100%) = 15% exists in this alternate calibration procedure. This error could be reduced by making a calibration card that would only be used for calibration. This card would be identical to the second card as shown in Figure 7.1 except that the standard logarithmic converter would be replaced with an EPROM programmed such that each one keV increment around 60 keV would fall in a different bin so that the amplifier gain could be set exactly. Note that since none of the analog circuitry would be on the calibration card, no error due to the temporary substitution of the regular card with the calibration card would exist. Then, to set the gain more accurately, the gain resistor on the amplifier moved to the shaper would be a potentiometer. The potentiometers should have glyptol applied to them after calibration. The above changes would greatly increase system accuracy.

The modifications of Section 7.3 reduce the pile-up problem since the only times that pile up affects measured data are if a second pulse occurs in the 2 μs interval after the first pulse and before the one shot following the comparator times out or if the shaper is still responding to a previous pulse at the beginning of a sample period. These probabilities are so low under any conditions envisioned as to not appreciably affect the data. However, if data is to be taken under extremely high flux rates and the measurement of high energetic particles is paramount, the pile-up could be reduced by replacing the shaper with an amplifier and a low-pass filter. The pile-up would be almost eliminated (although a low-pass filter spreads a pulse some), but other differences in high energy measurements would not be seen. However, the noise level would be higher, so the minimum energy measurable would rise.

APPENDIX I. Sampling Error*

I.1 *Definition of the Problem*

The design of the sample-and-hold system is such that it counts only the largest pulse (corresponding to the most energetic particle arriving at the detector) during the sampling interval. In situations of high flux this results in the count rate (or apparent flux) being less than the pulse rate (or actual flux).

It will be shown in this Appendix that, assuming that the pulses are Poisson distributed, a correction can be applied to the apparent flux to obtain the actual flux. In considering the sampling error we ignore the separate problem of possible overflow in the data storage system. The correction is somewhat different for the highest energy range (bin 15) than for the other energy ranges (bins 1 to 14) because the latter require a correction which involves all higher energy ranges. Thus the development of the correction begins with the highest energy range (bin 15).

I.2 *The Highest Energy Range*

If N is the average number of pulses during a sampling interval then the probability of n pulses occurring in a sampling interval is

$$P(n) = (N)^n e^{-N}/n! \qquad (I.1)$$

where n = 0, 1, 2 ... and 0! = 1.

By definition

$$\sum_{n=0}^{\infty} P(n) = 1$$

and, as expected, the average number of pulses per interval is

$$\sum_{n=0}^{\infty} nP(n) = N$$

Let N_{15} be the average number of pulses in a sampling interval for the highest energy range (bin 15). If, now, only one count is recorded when one or more pulses occur in a sampling interval the average number of counts per interval is

---

*This appendix by L. G. Smith

$$N'_{15} = \sum_{n=1}^{\infty} P(n) = 1 - e^{-N_{15}} \tag{I.2}$$

Note that, as expected, for $N_{15} \to \infty$, $N'_{15} \to 1$.

Since N'_{15} is the count rate measured in the experiment the actual pulse rate is

$$N_{15} = \ln\left(\frac{1}{1 - N'_{15}}\right) \tag{I.3}$$

From equation (I.2) the correction increases rapidly for $N_{15} > 1$. For $N_{15} = 3$, for example, $N'_{15} = 0.950$ and for $N_{15} = 4$, $N'_{15} = 0.982$. Thus a 3% error in determining the count rate gives a 25% error in the pulse rate. Taking $N_{15} = 3$ as a practical upper limit the corresponding pulse rate is $3/(150\ \mu s) = 2 \times 10^4\ s^{-1}$. It can be noted that this upper limit on pulse rate is comparable to that of the completely independent staircase system.

I.3 *Lower Energy Ranges*

First we consider the next lower energy range (bin 14). Pulses can be recorded in this range only if there were no pulses in the highest energy range during a particular sampling interval.

From equation (I.1) the probability of a sampling interval having no pulses falling in the highest energy range is

$$P(0) = e^{-N_{15}} \tag{I.4}$$

For example, if $N_{15} = 3$ pulses per sampling interval (on average) then 5% of the sampling intervals will have no pulses of the highest energy range (bin 15).

In addition, for the pulses of the next lower energy range (bin 14), there is again the possibility of multiple pulses in a sampling interval. If N_{14} is the average number of pulses per sampling interval in this energy range (bin 14) then the average number of counts per sampling interval is

$$N'_{14} = (1 - e^{-N_{14}})e^{-N_{15}} \tag{I.5}$$

In terms of the count rates N'_{14} and N'_{15} measured in the experiment the actual pulse rate for the energy range (bin 14) is, using equation (I.2),

$$N_{14} = \ln\left(\frac{1 - N'_{15}}{1 - N'_{14} - N'_{15}}\right) \tag{I.6}$$

Pulses can be recorded in the next lower energy range (bin 13) only if no pulses of the two higher energy ranges (bin 14 and 15) occurred. There is also the possibility of multiple pulses in a sampling interval. If N_{13} is the average number of pulses per sampling interval in this energy range (bin 13) then the average number of counts per sampling interval is

$$N'_{13} = (1 - e^{-N_{13}})e^{-(N_{14} + N_{15})} \tag{I.7}$$

In terms of the count rates N'_{13}, N'_{14} and N'_{15} measured in the experiment the actual pulse rate for the energy range (bin 13) is

$$N_{13} = \ln\left(\frac{1 - N'_{14} - N'_{15}}{1 - N'_{13} - N'_{14} - N'_{15}}\right) \tag{I.8}$$

Comparing equations (I.3), (I.6) and (I.8) shows the general form of the equation for the energy range specified as bin k is expected to be

$$N_k = \ln\left(\frac{1 - N'_{k+1} - \ldots N'_{15}}{1 - N'_k - N'_{k+1} \ldots N'_{15}}\right) \tag{I.9}$$

Thus all energy ranges can be corrected for the sampling error.

It follows from equation (I.9) that

$$\sum_{k=0}^{15} N'_k \leq 1 \tag{I.10}$$

Further consideration shows that if there are no counts in the lowest energy range (bin 0, which responds to system noise) then

$$\sum_{k=0}^{15} N'_k = 1 \tag{I.11}$$

This provides a useful check on the operation of the system. It makes the occurrence of data overflow immediately obvious and also allows an independent check of the total number of sampling intervals.

Table I.1 gives an illustration of the effect of sampling error for a total of 730 sampling intervals of 180 μs each, as in the instruments flown in the Energy Budget Campaign. The calculation assumes the actual pulse rate is the same in each energy bin, as would be the case for an exponential spectrum. (Recall that the ranges of the energy bins are assigned on a logarithmic scale). Thus, for a pulse rate of 556 s^{-1} (a total of 73 pulses)

Table I.1

Illustration of sampling error for 730 intervals

Pulses	73	146	365	730	1095	1460	2190	2920	3650	4380	5110	5840
N	0.1	0.2	0.5	1	1.5	2	3	4	5	6	7	8
15	69.5	132.3	287.2	461.4	567.1	631.2	693.7	716.6	725.1	728.2	729.3	729.8
14	62.9	108.3	174.2	169.7	126.6	85.4	34.5	13.1	4.9	1.8	0.7	0.2
13	56.9	88.7	105.7	62.5	28.2	11.6	1.7	0.3	-	-	-	-
12	51.5	72.6	64.1	23.0	6.3	1.6	0.1	-	-	-	-	-
11	46.6	59.5	38.9	8.5	1.4	0.2	-	-	-	-	-	-
10	42.1	48.7	23.6	3.1	0.3	-	-	-	-	-	-	-
9	38.1	39.9	14.3	1.1	0.1	-	-	-	-	-	-	-
8	34.5	32.6	8.7	0.4	-	-	-	-	-	-	-	-
7	31.2	26.7	5.3	0.2	-	-	-	-	-	-	-	-
6	28.2	21.9	3.2	0.1	-	-	-	-	-	-	-	-
5	25.6	17.9	1.9	-	-	-	-	-	-	-	-	-
4	23.1	14.7	1.2	-	-	-	-	-	-	-	-	-
3	20.9	12.0	0.7	-	-	-	-	-	-	-	-	-
2	18.9	9.8	0.4	-	-	-	-	-	-	-	-	-
1	17.1	8.0	0.3	-	-	-	-	-	-	-	-	-

in each energy bin, the average number (N) of pulses per sampling period is 0.1. In the absence of sampling error, each pulse would be sensed and each bin would record 73 pulses. Sampling error reduces the number progressively with decreasing bin number until, in energy bin 1, only 23.4% of the pulses are recorded.

As the average number of pulses per sampling interval increases the range of energies that can be measured decreases so that the energy spectrum can be established only for the higher energies. On the other hand this effect extends the range of count rates that the instrument can measure.

The expected counts are given in Table I.1 to tenths, based on the calculated probability. Only integral numbers of counts are recorded by the instrument.

APPENDIX II. Modifications to the Receiver

The radio propagation experiment uses Faraday rotation and differential absorption to measure electron density. The receiver is located within the payload, Figure 5.2. The signal is transmitted from the ground, near the launch site.

The receiver is a single conversion superheterodyne utilizing a 4 kHz wide ceramic filter (Vernitron TL-2D5A), an envelope AM detector, and AGC. The receiver was originally developed by G. W. Henry in the Aeronomy Laboratory in 1974 and is described on pages 51-64 of *Edwards* [1975]. The schematic used from 1974 until the Energy Budget Campaign is shown in Figure II.1.

II.1 *Receiver Changes*

The new experimental method differs from that used previously in that the nulls in the received signal must be accurately measured. The old AM detector had a residual output of 200 mV. Furthermore, this value was not consistent. These factors limited the capability to measure low amplitudes. The offset was due to leakage current in the germaniam detector transistor. This problem was eliminated by replacing the transistor detector with a hot carrier diode. The present schematic of the modified portion of the receiver is shown in Figure II.2. The value of C216 was decreased (decreasing the detector time constant) so that the output would follow the null more accurately.

The receiver's AGC did not operate smoothly. This was traced to high frequency regeneration in the two operational amplifiers and to AGC latch-up on momentary strong signals. The first problem, which is probably due to some very long leads in the PC board layout, was eliminated by adding 0.0047 μF capacitors directly across the IC's to reduce their high frequency response. The latch-up problem was eliminated by placing a 100 Ω resistor in series with C219 so that momentary large signals or a static burst will not fully charge the AGC.

II.2 *Further Recommended Receiver Changes*

The receiver has considerable spurious response as shown in Table 4.7 of *Ginther and Smith* [1975]. The spurious responses are largely due to images and to a nonlinear RF amplifier.

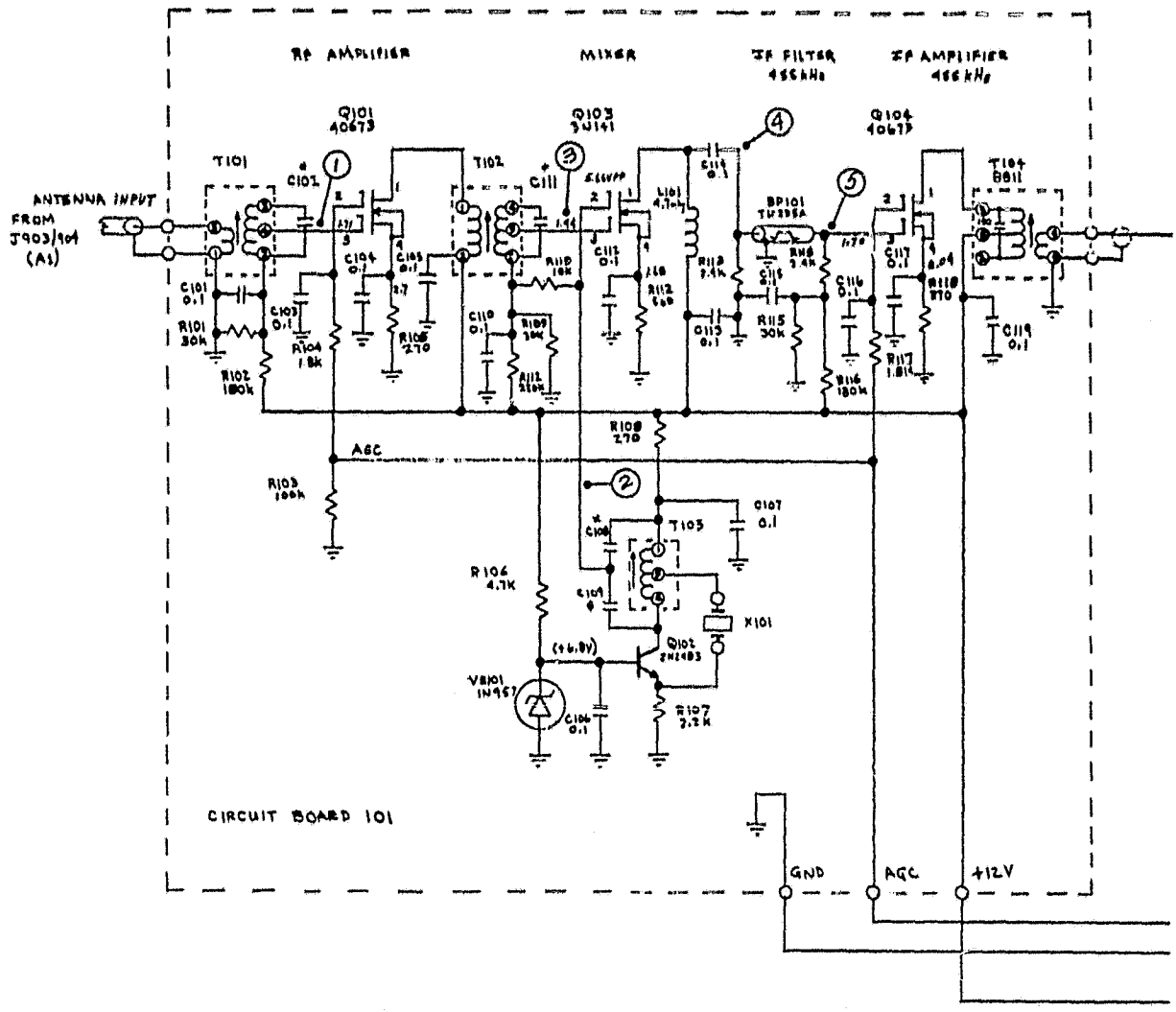

NOTES:

1. ALL RESISTORS 1/4 WATT

\# 2. THE FOLLOWING PART VALUES DEPEND UPON INPUT FREQUENCY:

C102	T101	Y101
C108	T104	
C109	T105	
C111		

3. THE BASE DIAGRAMS FOR THE TRANSFORMERS ARE:

(BOTTOM)

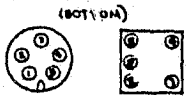

T101
T102
T103

T104
T201
T202

DA Receiver Schematic
IR 1274 D108064

Figure II.1 Circuit of the receiver used in the propagation experiment from 1974 to 1979. The circuit was modified for the Energy Budget Campaign, 1980.

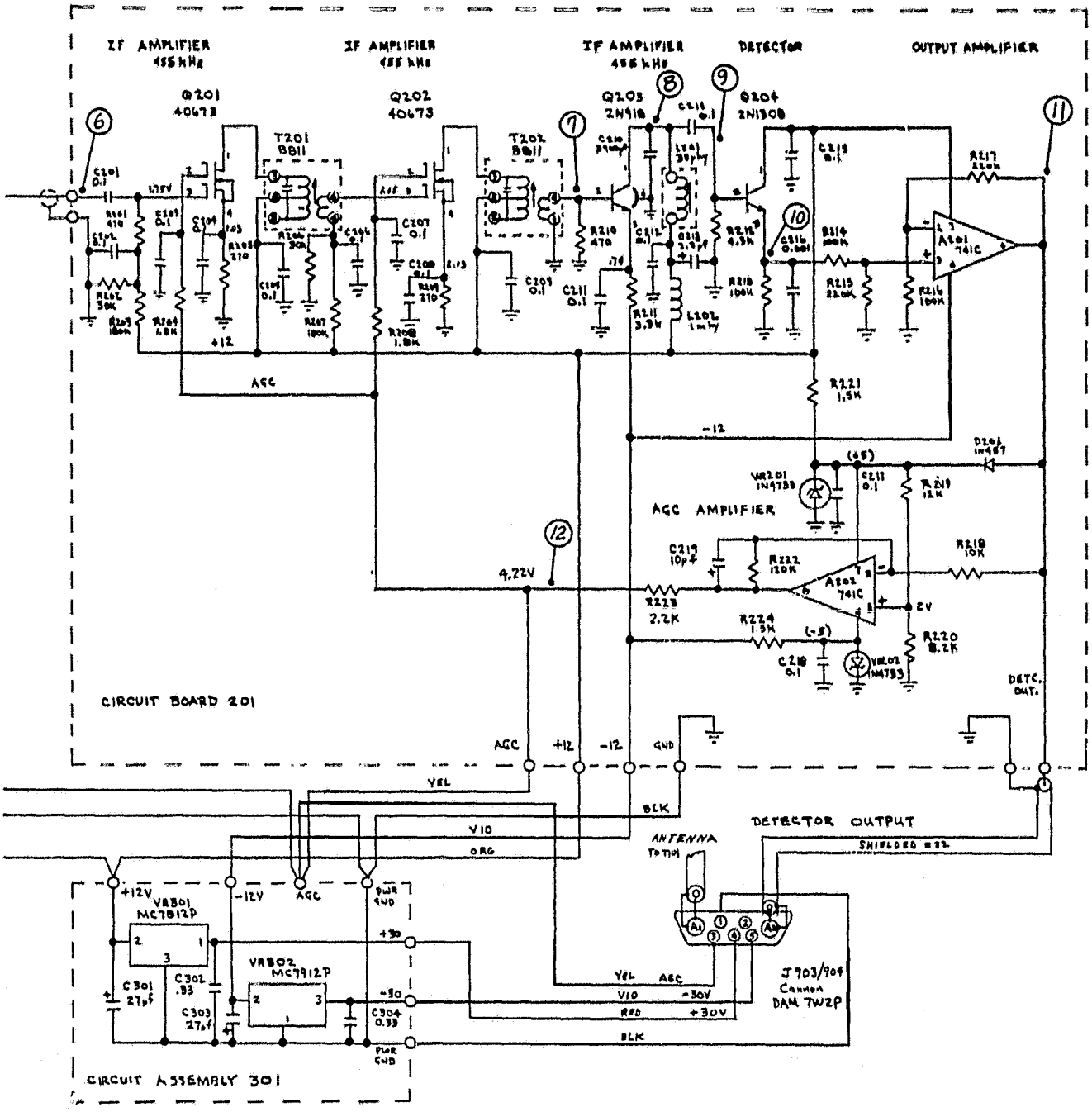

Figure II.1 (continued)

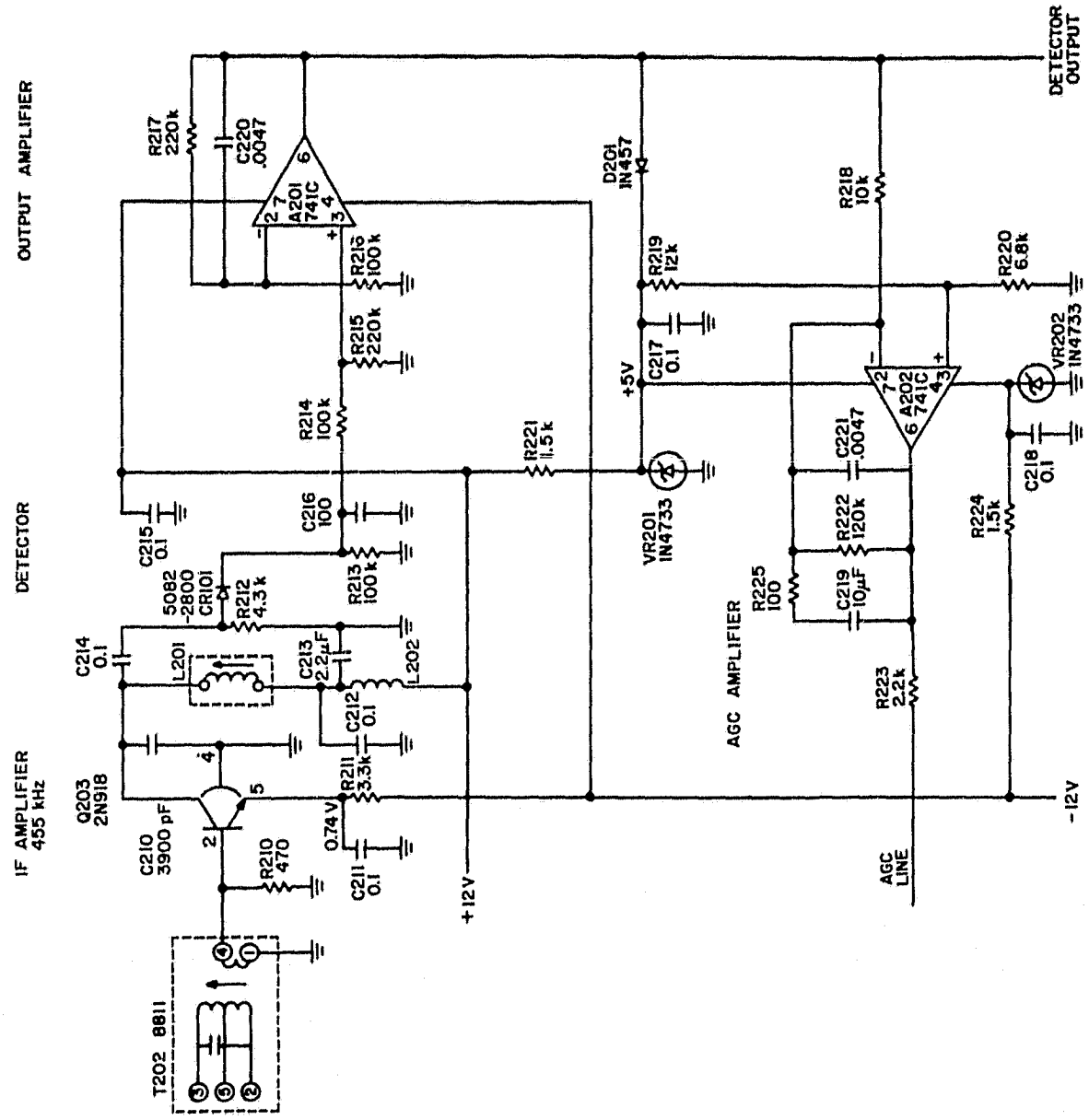

Figure II.2 Circuit showing modifications effected for the Energy Budget Campaign.

The images are due to the fact that the receiver is now being used at a much higher frequency (8 MHz) than it was originally designed for (2-5 MHz). The input tuned circuit is, consequently, not sharp enough to properly attenuate the image. Figure II.3 shows a solution to this problem. C120 and L102 are added to the input tuned circuit and are tuned to series resonance at the image frequency. The value to C102 is changed to compensate for the reactance of C120 and L102 at the desired frequency.

The nonlinearity of the RF amplifier is due to the use of a FET for the first amplifier. The use of a "square law" device for an RF amplifier that should have low spurious response is undesirable. The device choice is also poor when intermodulation distortion performance is considered. Such an amplifier should only be used after a filter to eliminate exposure of the amplifier to the spurious frequencies. This problem can be eliminated by replacing the FET with a BJT. The IF amplifiers, which are protected by the filter, are examples of the proper use of FET's in receiver design.

AGC should be removed from the RF amplifier in order to minimize the receiver noise figure. This will cause the receiver to saturate on the launch pad, but will improve its performance on weak signals during the flight.

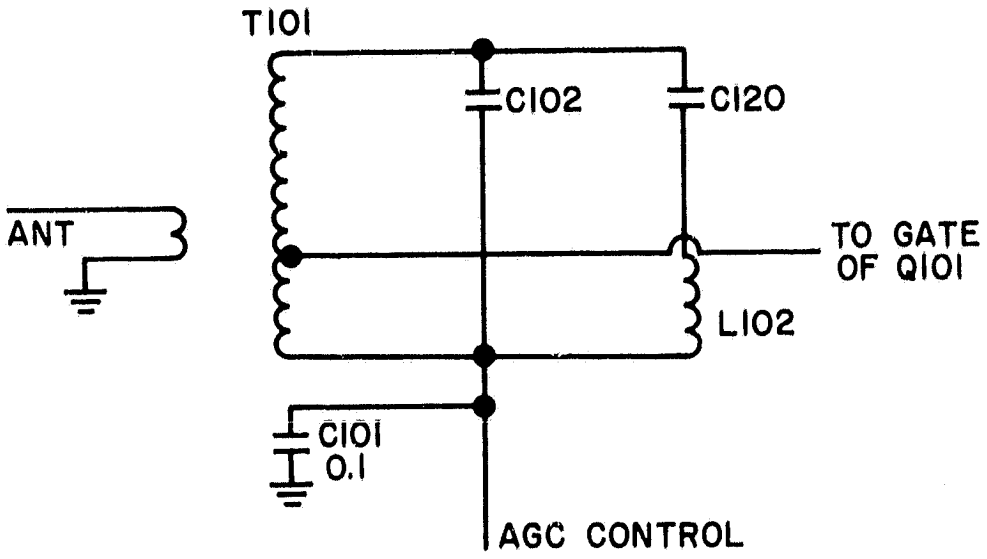

Figure II.3 Recommended circuit to improve image rejection.

REFERENCES

Braswell, F. M. and L. G. Smith [1981], A rocket-borne microprocessor-based experiment for investigation of energetic particles in the *D* and *E* regions, *Aeron. Rep. No. 96*, Aeron. Lab., Dep. Elec. Eng., Univ. Ill., Urbana-Champaign.

Davis, L. L., L. G. Smith and H. D. Voss [1979], A rocket-borne data-manipulation experiment using a microprocessor, *Aeron. Rep. No. 84*, Aeron. Lab., Dep. Elec. Eng., Univ. Ill., Urbana-Champaign.

Edwards, B. [1975], Research in Aeronomy: October 1, 1974 - March 31, 1975, *Prog. Rep. 75-1*, Aeron. Lab., Dep. Elec. Eng., Univ. Ill., Urbana-Champaign.

Fries, K. L., L. G. Smith and H. D. Voss [1979], A rocket-borne energy spectrometer using multiple solid-state detectors for particle identification, *Aeron. Rep. No. 91*, Aeron. Lab., Dep. Elec. Eng., Univ. Ill., Urbana-Champaign.

Gilchrist, B. E. and L. G. Smith [1979], Rocket measurement of electron density in the nighttime ionosphere, *Aeron. Rep. No. 85*, Aeron. Lab., Dep. Elec. Eng., Univ. Ill., Urbana-Champaign.

Ginther, J. C. and L. G. Smith [1975], Studies of the differential absorption rocket experiment, *Aeron. Rep. No. 64*, Aeron. Lab., Dep. Elec. Eng., Univ. Ill., Urbana-Champaign.

Leung, W., L. G. Smith and H. D. Voss [1979], A rocket-borne pulse-height analyzer for energetic particle measurements, *Aeron. Rep. No. 83*, Aeron. Lab., Dep. Elec. Eng., Univ. Ill., Urbana-Champaign.

Voss, H. D. and L. G. Smith [1974], Design and calibration of a rocket-borne electron spectrometer for investigation of particle ionization in the nighttime midlatitude E region, *Aeron. Rep. No. 62*, Aeron. Lab., Dep. Elec. Eng., Univ. Ill., Urbana-Champaign.

Voss, H. D. and L. G. Smith [1980], Global zones of energetic particle precipitation, *J. Atmos. Terr. Phys.*, *42*, 227-239.